ADVANCED MATERIALS
www.advmat.de

Toward the Commercialization of Perovskite Solar Modules

Pengchen Zhu, Chuanlu Chen, Jiaqi Dai, Yuzhen Zhang, Ruiqi Mao, Shangshang Chen, Jinsong Huang,* and Jia Zhu**

Perovskite (PVSK) photovoltaic (PV) devices are undergoing rapid development and have reached a certified power conversion efficiency (PCE) of 26.1% at the cell level. Tremendous efforts in material and device engineering have also increased moisture, heat, and light-related stability. Moreover, the solution-process nature makes the fabrication process of perovskite photovoltaic devices feasible and compatible with some mature high-volume manufacturing techniques. All these features render perovskite solar modules (PSMs) suitable for terawatt-scale energy production with a low levelized cost of electricity (LCOE). In this review, the current status of perovskite solar cells (PSCs) and modules and their potential applications are first introduced. Then critical challenges are identified in their commercialization and propose the corresponding solutions, including developing strategies to realize high-quality films over a large area to further improve power conversion efficiency and stability to meet the commercial demands. Finally, some potential development directions and issues requiring attention in the future, mainly focusing on further dealing with toxicity and recycling of the whole device, and the attainment of highly efficient perovskite-based tandem modules, which can reduce the environmental impact and accelerate the LCOE reduction are put forwarded.

1. Introduction

Since first employed as sensitizers in dye-sensitized solar cells (DSSCs), organic–inorganic hybrid perovskites have emerged as one of the most attractive light-harvesting materials.[1,2] With the rapid development, single-junction PSCs have exhibited a certified power conversion efficiency (PCE) of 26.1%, showing promising potential in the photovoltaic (PV) field.[3] To date, the record-high PCEs are merely realized on small-size PSCs (≈0.1 cm^2), while the development of large-area PSMs still lags.[4,5] Systematic investigations and a comprehensive understanding of PSMs are urgently needed for their ongoing commercialization process. In the beginning, we believe it is essential to reach a consensus on the terms: "cell" and "module" for the following discussion. According to the National Renewable Energy Laboratory (NREL) Champion Photovoltaic Module Efficiency Chart, the size of a typical solar module should exceed 200 cm^2 and can be further subdivided into four categories: 200–800 cm^2 (submodule), 800–6500 cm^2 (small module), 6500–14 000 cm^2 (standard module), >14 000 cm^2 (large module).[6] The NREL definition focuses primarily on the industrial consideration where no standards have been set for sizes below 200 cm^2. However, for the perovskite PV community particularly from the academic community, the areas of reported modules are often below 200 cm^2. Thus, a complementary definition by Green et al. can be considered at this stage that a PV device with an area exceeding 1 cm^2 can be called a cell and the sizes between 10–200 cm^2 can be called a minimodule.[7,8] Here, we combine these two standards to give a comprehensive definition, the details of which can

P. Zhu, C. Chen, J. Dai, Y. Zhang, R. Mao, J. Zhu
National Laboratory of Solid State Microstructures
School of Sustainable Energy and Resources
Jiangsu Key Laboratory of Artificial Functional Materials
Frontiers Science Center for Critical Earth Material Cycling
Nanjing University
Jiangsu 210023, P. R. China
E-mail: jiazhu@nju.edu.cn

S. Chen
State Key Laboratory of Coordination Chemistry
MOE Key Laboratory of High-Performance Polymer Materials & Technology
School of Chemistry and Chemical Engineering
Nanjing University
Nanjing, Jiangsu 210023, P. R. China
E-mail: schen@nju.edu.cn

The ORCID identification number(s) for the author(s) of this article can be found under https://doi.org/10.1002/adma.202307357

DOI: 10.1002/adma.202307357

J. Huang
Department of Applied Physical Sciences
The University of North Carolina at Chapel Hill
Chapel Hill, NC 27599, USA
E-mail: jhuang@unc.edu

J. Huang
Department of Chemistry
The University of North Carolina at Chapel Hill
Chapel Hill, NC 27599, USA

J. Zhu
College of Engineering and Applied Sciences
Nanjing University
Nanjing, Jiangsu 210023, P. R. China

Table 1. Size criteria are defined by the Solar Cell Efficiency Table and NREL chart and the combined size criteria used in this manuscript.

Size [cm^2]	Criteria (by Green et al.)	Size [cm^2]	Criteria (by NREL)
>1	Single-junction cell	200–800	Submodule
10-200	Minimodule	800–6500	Small module
200–800	Submodule	6500–14 000	Standard module
>800	Small module	>14 000	Large module
Size (cm^2)	Combined criteria		
≤1	Small cell		
1–10	Cell		
10–200	Minimodule		
200–800	Submodule		
800–6500	Small module		
6500–14 000	Standard module		
>14 000	Large module		

be found in **Table 1**. For convenience, we also define the devices with an area below 1 cm^2 as small cells consistent with the previous literature.[6–8]

In this review, we first introduce the current status of perovskite PV devices and then identify their potential applications and critical commercialization challenges. We then focus on how to overcome these extant challenges, including developing strategies to fabricate high-quality films over a large area and further improve PCEs and stability for commercial demands. To expound on the points, the following sections include an introduction to device configurations, scalable deposition methods, strategies to improve film qualities, cost evolution, and life cycle assessment. In the final, we propose some potential issues and developing directions for the future.

2. Current Status of Perovskite PV Devices

The golden triangle is commonly used to evaluate the feasibility of the commercialization of PV technologies, including PCEs, lifetime (or stability), and cost (**Figure 1a**).[9] A combination of these factors contributes to an ultimate measurement index, the LCOE, which reveals the average net cost of electricity generation for an electricity generator over its lifetime.[9,10] There are no very strict industrial demands of these parameters in PV fields, but for emerging PV technologies toward commercialization, they should have an LCOE comparable to the state-of-the-art analogs, for example, the LCOE at the utility-scale is ≈5 ¢ kWh^{-1} for crystalline silicon (c-silicon or c-Si) modules in 2020.[11] A relatively rough comparison of the three parameters between perovskite and commercially used c-silicon PV devices is shown in Figure 1b, where the lower module efficiency and poor stability are two primary constraints currently.[9,12–14] Assuming a daily insolation time of ≈6 h, the 10 000-hour continuous operation time of a PSM is roughly equivalent to a lifetime of ≈4.5 years in real-world conditions.[12] The PCE of a perovskite standard module is now reaching 18.2% at an area of 7200 cm^2 while the 24.7%-Si standard module is realized at an area of 17806 cm^2.[6,13,14] Besides, according to the calculation by NREL, the minimum sustainable price (MSP, defined as the price that provides the minimum rate of return necessary in a given industry to support a sustainable business over a long term) with a 15%-gross margin of PSMs manufactured at a small scale is calculated to be 0.38 \$ W^{-1}, higher than that of c-Si (0.25–0.27 \$ W^{-1}), but it is with possible reductions to 0.21 \$ W^{-1} for a larger scale if PCE can be improved to 22% for a single-junction PSM without incurring additional costs.[10,11] Further developing an all-perovskite two-junction tandem module with a PCE of 30% could lower the cost to 0.18 \$ W^{-1} in the future. Detailed processing flow for sheet-to-sheet PSMs and assumptions used for these cost calculations are presented in Figures S1,S2 and Table S1 (Supporting Information),[11] which will be further discussed in the following sections.

During the past few years, tremendous efforts have been devoted to the investigation of perovskite PVs and remarkable development has been achieved at both cell and module levels.[1–6] Since the first demonstration of a $CH_3NH_3PbI_{3-x}Cl_x$-based perovskite minimodule with a PCE of 5.1%,[15] perovskite small modules now have achieved a certified PCE of 19.5% with a designated illumination area of 810.1 cm^2.[13,14] The basic structures of PSMs are similar to PSCs, which can be classified into n-i-p (conventional) and p-i-n (inverted) structures, according to their different stacking orders (Figure S3, Supporting Information). Considering the significantly increased resistance loss over the large-area transparent conducting oxide (TCO) electrodes, PSMs are not simply equal to the proportional magnification of the small-area devices and need to be divided into smaller sub-cells through series or parallel connections, similar to cadmium telluride (CdTe) and copper indium gallium selenide (CIGS).[4,10,11] Areas that occupy the module but do not contribute to electricity generation are defined as dead areas. To quantify the utilization, the ratio between the photoactive area and the combined area (the sum of active and dead area) is usually referred to as the geometric fill factor (GFF).[5,11] These make the area defined in a module more complex, including active, designated illumination, aperture, and total areas (Figure S3, Supporting Information).[16] Here, we strongly recommend reporting the PCEs along with the corresponding areas and GFF, giving a unified comparison with other reported results. PCEs of some typical perovskite PV devices concerning the areas are shown in Figure 1c and Table S2 (Supporting Information), where the classification is according to the fabrication methods of perovskite films (discussed later).

Except for the PCE development, the stability issue, another primary commercialization concern, has also experienced rapid progress. To date, stability evaluation standards have not been expressly set for perovskite PVs, and these tests were often performed under various situations. Now, employing the existing criteria (e.g., accelerated tests in International Electrotechnical Commisson (IEC) 61215 and International Summit on Organic Photovoltaic Stability (ISOS) protocols) for evaluation is being accepted by industry and academia.[16–18] IEC 61215 is an industry-standard for certification of silicon PV technology for commercial deployment, while ISOS provides guidelines on stability testing under accelerated conditions to enable comparison across various reports.[16–18] Several companies and research groups have announced passing partial or complete accelerating aging tests like damp-heat, and temperature cycles in IEC 61215, demonstrating the stability potential to meet the commercial requirements.[16,17,19,20] These accelerated tests are designed to correlate the real-world lifetime to the values obtained in the

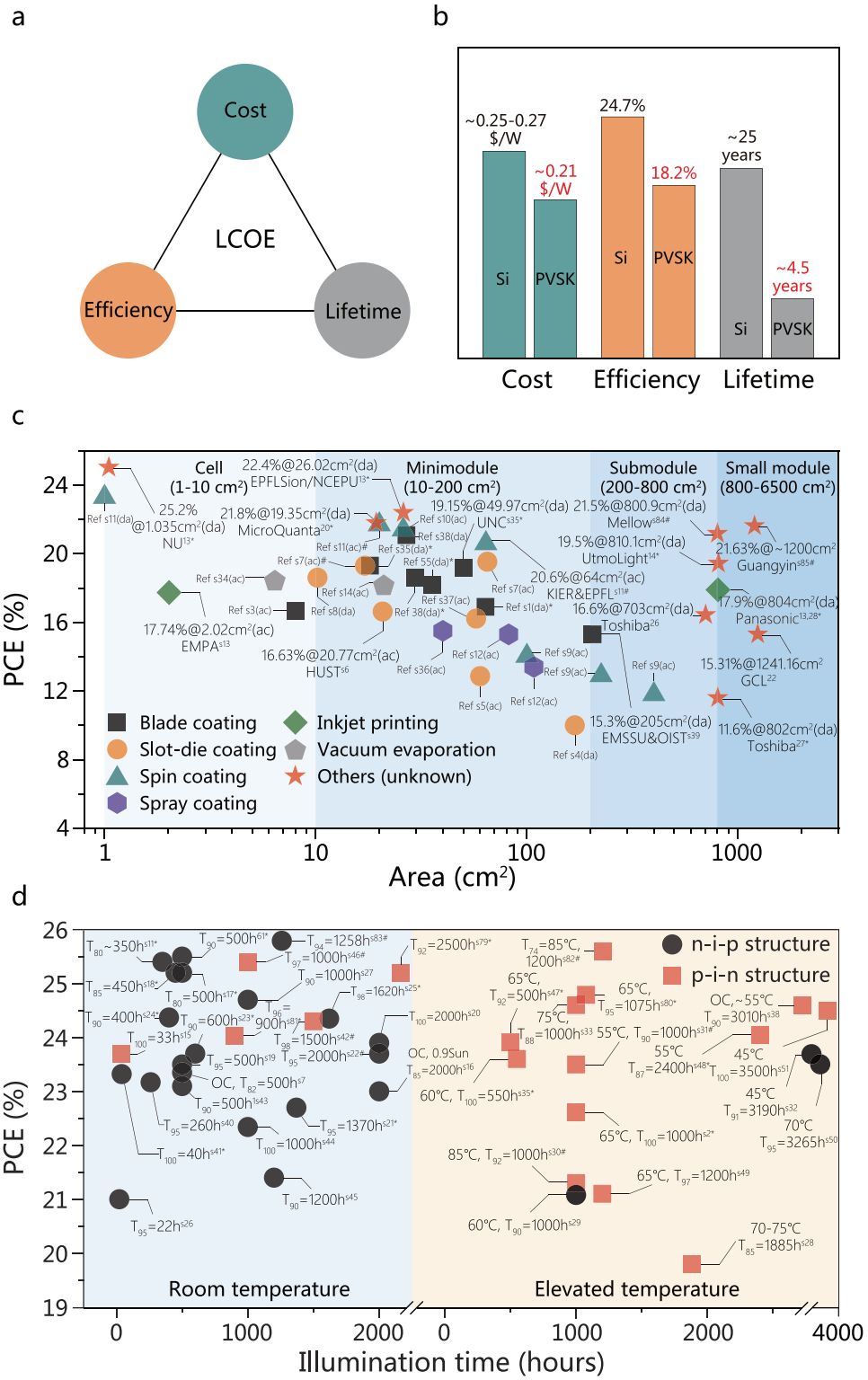

Figure 1. Current status of perovskite PV devices. a) Golden triangle in photovoltaic community. b) Comparison of cost, efficiency, and lifetime between silicon modules and single-junction PSM. c) Typical PCEs from cells to modules with respect to device areas. Da: designated areas, ac: active areas. * and # denote the certified PCEs at stabilized and unstabilized measurements. d) Typical stability of perovskite solar cells under continuous illumination. The PCEs are the best values from the reports. S denotes the references in the Supporting Information. OC denotes the open-circuit conditions while other devices were measured at maximum power point (MPP) conditions. $T_{xx} = Y$ h means that the PECs drop to *xx*% of the initial value after *Y*-hour aging.

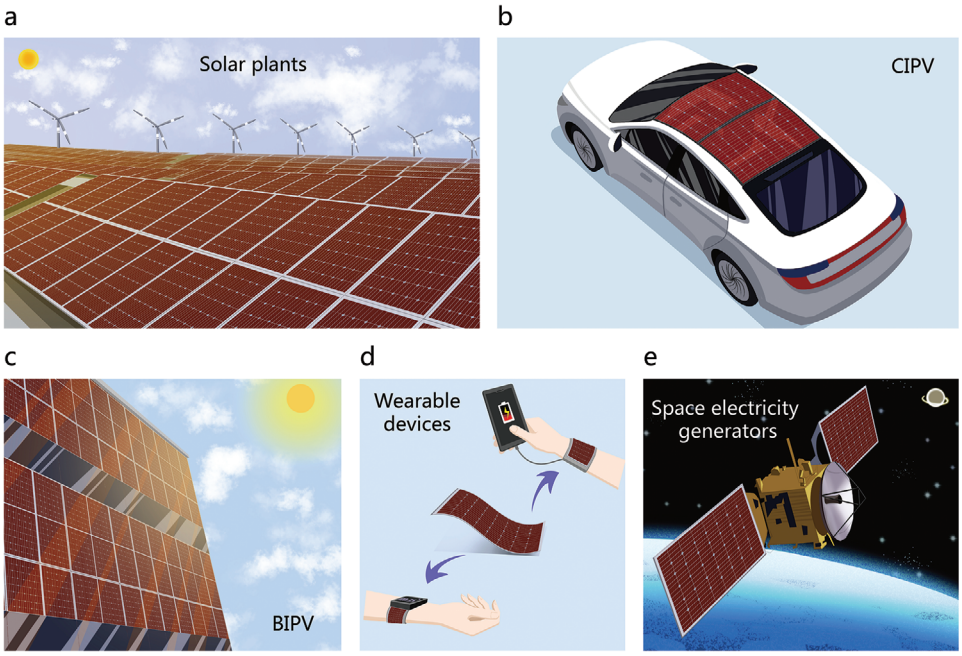

Figure 2. Potential applications of PS. a) Solar plants. b) CIPV. c) BIPV. d) Wearable flexible electronics. e) Electricity generators in satellites or space shuttles.

laboratory, but the experience from the silicon and thin-film PV industry has demonstrated that these tests are insufficient to predict the lifetime under real-world conditions.[11] For example, PV modules passing IEC standards do not always meet a lifetime exceeding 20 years.[11,16] Thus, the long-term field test of PSMs under outdoor conditions which accurately reflects the practical performance evolution of PSMs, is of vital importance.[4,11,17] In general, although the stability evaluation varies, we believe illumination stability is still a valuable consideration. A photostability summary of typical perovskite PV devices is plotted in Figure 1d, which focuses on the cell level due to the relatively limited module stability reports. Some typical results under other types of stability tests, such as thermal cycle, damp heat, and humidity freeze are summarized in Table S3 (Supporting Information).

Compelling progress in the perovskite PV field has attracted massive investments, sparking a string of start-ups and new divisions within established PV companies (**Table 2**).[13,14,20–31] However, a big gap between the current status and commercial PV technologies still exists, especially the gap in the device's lifetime even compared to other thin-film technology. For example, First Solar, a CdTe PV manufacturer, has announced the industry's lowest degradation rate of 0.2%, which means more than 90% of the original power output will be maintained at the end of the panels' 30-year performance warranty.[30]

3. Potential Applications and Remaining Challenges

3.1. Potential Applications

Due to additional advantages like light-weight, tunable transparency and color, compatibility with flexible or curved substrates, and excellent weak-light response, PSMs can set more potential applications as well as the mainstream scenes like solar plants or building applied photovoltaics.[2,32] For instance, some attempts at building-integrated photovoltaics (BIPV), car-integrated photovoltaics (CIPV), wearable or portable electronics, in-door electricity chargers, etc. are significantly promising and need further exploration (**Figure 2**). What's more, the high power-per-weight characteristic, along with the excellent stability under harsh irradiation, may render PSMs to have the potential to surpass those state-of-the-art III-V semiconductor-based PVs like gallium arsenide (GaAs) as electricity converters in space.[30,33] Better tolerance to high-energy particles in a space environment (such as electron and proton beams) of perovskite PV devices has been proven than those of Si- and GaAs-based cells, mainly due to the high defect tolerance and self-healing properties.[33] Here, taking BIPV as an example, we classify some unique characteristics of perovskites in this application. According to previous reports, the BIPV market is projected to be ≈€11 billion with 16 GW of power installed in 2021 and is expected to grow at an annual growth rate of 40% in the next decade.[32,34] As one of the important parts of BIPV, solar windows require not only energy generation but also color appearance and transparency for scenic viewing and lighting control, which is hard to realize in mainstream c-Si-based technology. From this aspect, perovskites' unique advantages, including feasible color tunability from the semi-transparency and bandgap tunability, and higher efficiency, make them promising candidates in the BIPV markets. In addition to BIPV, some other prototypes have been already demonstrated for practical use and field tests. A panel with a total area of 4.5 m^2, integrated by nine large-area (0.5 m^2) perovskite solar panels was demonstrated in a stand-alone solar farm. It exhibited a peak power exceeding 250 W in real-world conditions, proving the scalability of the feasibility of perovskite technology.[35] Recently, one perovskite PV system realized by Microquanta

Table 2. Companies exploring the development and commercialization of perovskite single-junction modules.

Company	Founded	Technologies	Performance claims	Stability claims	Industrial progress claims
Microquanta Semiconductor	2015	Single-junction perovskite modules on rigid glass.	Certified 21.8%-perovskite minimodule (19.35 cm^2) in 2022.[20]	Perovskite standard modules passed all the tests in IEC 61215, and IEC 61730 in 2023.[20]	The first batch of 5000 pieces of standard modules (1245 mm × 635 mm, 115–130 W $piece^{-1}$) has been delivered to customers in 2022.[20] The world's first commercial perovskite terrestrial photovoltaic power station (1 MW) was successfully connected to the grid in November 2023.[20]
Wuxi Utmolight Technology	2020	Single-junction perovskite modules on rigid glass.	Certified 19.5% (stabilized)-perovskite submodule (810.1 cm^2) in 2023. Certified 18.2% -perovskite standard module (0.72 m^2) in 2023.[13,14]	Perovskite standard modules (0.72 m^2) passed all the tests in IEC 61215, and IEC 61730 in November 2023.[14]	A 150-MW production line has been put in production in 2022 and a 1-GW production line has been put in production in 2023.[14]
Kunshan GCL Optoelectronic Material	2019	Perovskite modules on rigid glass. A slot-die deposition method of perovskite was claimed.	Certified 15.31%-perovskite small module (1241.16 cm^2) in 2019. Certified 18.04%-perovskite large module (2 m × 1 m) in 2023.[22]	Undisclosed.	A 100-MW production line has been put in trial production in 2021, where the size of the module is 2 m × 1 m.[22]
WonderSolar	2016	All printable perovskite modules.	12.5%- perovskite minimodule (100 cm^2).[23,24]	A PSC worked for more than 9000 h at the MPP condition (≈55 °C) without obvious decay in 2020.[17]	Demonstration of perovskite small modules with areas of 3600 cm^2.[23,24] The construction of the second large (trial) production line of 200 MW printable mesoscopic perovskite solar panels began in June 2023.[23]
Toshiba	1875	Perovskite modules on rigid and flexible substrates. A meniscus coating method was claimed.	Certified 11.6%- perovskite small module on rigid substrates (802 cm^2) in 2018 and 16.6%-perovskite submodules on flexible substrates and (703 cm^2) in 2023.[25–27]	Undisclosed	Undisclosed
Panasonic	1918	Perovskite modules on rigid glass. An inkjet printing method was claimed.	Certified 17.9%-(stabilized) perovskite small module (804 cm^2) in 2020.[23,28]	Undisclosed	Undisclosed
Saule Technologies	2014	Fully printed flexible, lightweight perovskite modules.	17%-PSCs and 10%-perovskite minimodules (100 cm^2). 30.9%-flexible perovskite small cells under 1000 lux in 2022.[24,31]	A small cell kept 84% of its initial efficiency after 1000 h at the MPP condition (0.6 suns) and lost no performance after 1000 h at 85 °C in 2022.[24,31]	Undisclosed
Solaronix SA	1993	Perovskite modules integrated into the building.	14.9%-PSCs (1cm^2) and 12% perovskite minimodule (100 cm^2).[24,29]	Undisclosed	Undisclosed

Semiconductor was combined with aquaculture and successfully connected to the power grid, representing an innovative application in the perovskite PV fields.[20]

3.2. Remaining Challenges

For commercialization, the LOCE of a nascent PV technology should be reduced to a comparable level with the existing ones, by demonstrating a higher PCE, longer lifetime, and lower manufacturing cost. Currently, PSMs have PCEs exceeding 20% but still with areas mostly below 100 cm^2.[9,10] Small modules will increase the fabrication cost and electrical loss, leading to a high LCOE and application restriction. A trend for the module to get larger appears in the consideration of cost reduction but sometimes increases the transport/installation difficulties and causes safety concerns. The currently commercial thin-film CdTe modules possess typical sizes like 1.2 m × 0.6 m, which can serve as a proper guideline for perovskites.[11,36] Thus, the first challenge of perovskite commercialization is to scale up the module size without sacrificing their PCEs, through developing reproducible and scalable deposition strategies for high-quality films.[4,5] To meet a competitive LCOE with c-Si modules, a lifetime of 15 years is suggested to be the threshold for PSMs with an initial PCE of 19% based on Meng et. al.'s calculation.[9] Therefore, the second major challenge is the long-term stability of PSMs to ensure durable operation, especially compared to a 20–30-year lifespan of c-Si and CdTe. One crucial aspect before these is to develop a consensus on the stability test protocols, which often include accelerated aging tests to roughly predict the module lifetime.[18,37] In addition, cost reduction also needs increased attention. The manufacturing cost of PSMs calculated by NREL at a small scale is higher than that of silicon panels (≈0.38 \$ W^{-1} vs ≈0.25 \$ W^{-1}) but with possible reductions when increasing the production capacity.[11,18,19] Finally, to make the situation worse, these best values of PCE, stability, and cost cannot often be realized on one specific device, simultaneously. For example, the highly efficient perovskite devices are mostly based on a conventional structure and employ unstable spiro-OMeTAD with hygroscopic additives, which makes it hard to meet the stability demand. To further improve device stability, spiro-OMeTAD would be substituted by PTAA, but the latter contributes to a lower device PCE.[2,4,5]

4. Deposition Methods of Perovskite Modules

4.1. Perovskite Film Deposition

PSMs consist of several stacking layers, where the perovskite layer is the most vital part. To avoid short circuits, enable sufficient absorption, and facilitate charge transfer, uniform and compact perovskite film with high crystallinity is desired. The non-uniformity over large areas and large precursor waste render spin-coating (commonly used for PSCs) unacceptable in industrial manufacture. Scalable deposition methods include but are not limited to blade-coating, slot-die coating, spray coating, inkjet printing, screen printing, electrodeposition, physical vapor deposition (PVD), and chemical vapor deposition (CVD) (Figure S4, Supporting Information).[4,5,38–41]

Blade coating is an efficient meniscus deposition method for relatively small areas and is hard to transfer to industrial manufacturing due to its manual solution addition. One potential replacement is slot-die coating because it solves the issue of ink supply by the use of an ink reservoir.[38,41] The precursor ink flow is continuously squeezed from the thin slit to the substrate to form wet films first. To guarantee a considerable output, the deposition process should be controlled in the so-called Landau–Levich flow regime, where the film thickness increases with the increased moving speed.[40] In 2021, Toshiba Corporation's so-claimed perovskite submodule with a PCE of 15.1% (703 cm^2) was realized through a modified meniscus coating method.[26] Spray-coating is a low-cost solution deposition technique and involves droplet generation, transport, coalescence, and thin-film drying processes.[42] The most crucial part of morphology control is the ink surface tension, as it affects the contact angle of the droplets with the surface and facilitates the ink merging before the solvent evaporation. However, the re-dissolving issue that new-arrival wet ink will dissolve the as-formed film frequently occurs, where parameters like temperature, distance, and solvent kinds should be precisely adjusted.[42] Inkjet printing, a material-conserving technique used for dispersed or dissolved materials, enables rapid and large-area film formation.[43] The operating principle of inkjet is based on the ejection of fixed ink quantities in the form of droplets from nozzles, similar to spray deposition to some degree. The most common inkjet modes today are continuous inkjet printing and drop-on-demand printing, where the latter generates a single drop when required and enables material savings.[43] The Panasonic Corporation's small module with a high PCE of 17.9% (804 cm^2) was claimed through an inkjet method.[28]

Several other strategies also aim to form high-quality perovskite films. The screen-printing method uses a patterned mesh screen to hold and transfer ink to the substrates.[17,44] Recently, a breakthrough was made where the stable and viscosity-adjustable perovskite ink prepared from an ionic liquid solvent enabled screen-printing deposition regardless of humidity. Most notably, fully screen-printing devices with a single machine in ambient air were further successfully explored, exhibiting high PCEs at different sizes.[44] It has opened up new paths for the industrial fabrication of PSMs. Vapor-phase deposition, including PVD and CVD, is also commonly utilized.[45,46] PVD refers to the deposition where a perovskite or its precursor is directly evaporated to form a thin film, whereas CVD refers to the process where the lead halide is converted into perovskites by organic halide vapor. Compared to solution deposition, vapor-phase deposition produces highly uniform films but the low output and high technique expense might increase difficulties in commercialization.[44,45] The typical PCEs of PSMs where the perovskite layers adopt different deposition methods are plotted in Figure 1c for an intuitive comparison.

4.2. Other Layer Deposition

Like perovskite layers, the deposition of other layers can be typically classified into solution and vapor-phase methods. Soluble or dispersible materials such as poly[bis(4-phenyl)(2,4,6-trimethylphenyl)amine (PTAA), self-assembly monolayers

(SAMs), and metal oxide nanoparticles (tin oxide (SnO_2), titanium oxide (TiO_2)) can be deposited through solution methods while other materials like insoluble organic compounds and inorganic oxide can adopt vapor-phase depositions. To ensure uniformity, especially for layers with thickness down to several nanometers, vapor-phase-based methods are highly recommended. For example, high-quality nickel oxide (NiO_x) films can be achieved by magnetron sputtering and uniformly thin C_{60}/bathocuproine (BCP) layers can be achieved by thermal evaporation.[4,19] In addition, some soluble materials, like SAMs can also adopt vacuum deposition to guarantee an improved film homogeneity.[48] The front TCO and rear metal contacts are usually deposited in a vacuum, such as through magnetron sputtering or CVD. Carbon pastes, a low-cost rear electrode, can serve as a hole extractor in hole transporting layer (HTL)-free devices due to its carrier selectivity and are commonly deposited by solution methods like screen printing. Compared to metal electrodes, carbon materials are stable, inert to ion migration, and inherently water-resistant, serving as one promising alternative to overcome the stability issue. Although devices based on carbon electrodes lag behind those using metal electrodes due to the moderate hole extraction ability, energy mismatch, and limited lateral conductivity, they possess the potential for entirely R2R fabrication of perovskite devices.[49] In addition, the replacement by carbon will also mitigate the use of rare contact metals which will be further discussed in the following.[17,49]

5. Strategies to Improve PCEs of Perovskite Modules

To improve the module PCE, the first consideration is the formation of large-area layers with uniform morphology and superior electronic properties, especially for perovskite films. The second is the realization of optimal module design, including the sub-cell width, GFF, line width, electrodes, etc., which could bring in additional transport and optical loss when sub-cells are connected.[50,51] Before this discussion starts, we think it essential to have a brief introduction to the substrates employed in the perovskite cells and modules, which could have an impact on the device's performance.

5.1. Different Types of Substrates

The most commonly used substrates for perovskite PSMs are rigid glasses with TCO electrodes, which deliver the highest efficiency and scaling compatibility.[53–58] Other types of substrates, including ultra-thin glass, polymers, and metallic foils also exhibit potential for various applications.[57,58] Ultra-thin glass with a typical thickness of 100 µm possesses the combined merits of flexibility and a perfect hermetic protection barrier.[57,58] The bendability enables it to be adaptable in roll-to-roll manufacturing processes but the unsatisfactory mechanical properties bring in easy breaks. Polymeric substrates like polyethylene terephthalate (PET) and polyethylene naphthalate (PEN) are mainstream for flexible devices, which deliver better bendability, and lightweight properties compared to rigid and ultra-thin counterparts. However, the moderate transmission, coefficient of thermal expansion (CTE) mismatch between TCO and polymers, and high vapor penetration cause a lagged device performance when compared to commonly used rigid ones. Metallic foils like stainless steel, titanium, and copper (Cu) overcome the shortcomings of polymers partially, delivering high conductivity, excellent mechanical stability, and high tolerant temperature. However, the biggest obstacle of metal substrates for further development is their opacity, which proposes strict demands for top electrodes that need high transparency and conductivity simultaneously.[58] A comparison between different substrates regarding their features is summarized in Table S4 (Supporting Information) for reference.

5.2. Morphology Control of Each Layer

Each layer in the module should reveal a dense and uniform morphology regardless of different thicknesses. For bottom charge transport layers (CTLs) on TCO, the thickness is usually down to several nanometers, and in this case, solution methods face difficulties in forming such dense morphologies, especially on rougher substrates.[4,5,8] For example, the SAMs usually possess better quality on the smooth indium tin oxide (ITO) substrates than rough fluorine-doped tin oxide FTO. In addition, the wetting properties of the substrates will affect the deposition quality of the CTLs, thus, surface treatment like plasma and ultraviolet (UV)-ozone will assist in solving this problem and spreading the solution.[4,5] For the top CTLs on perovskite layers, this deposition issue by solution still exists as the roughness of perovskite could be up to tens of nanometers. To enable smooth top layers with high coverage, vacuum deposition is supposed as a superior alternative. For example, dense BCP film with 5–8 nm could be uniformly formed on rough perovskite by a thermal evaporation method.[38,40]

Solution methods seem to be mainstream due to the convenience and considerable output in deposition with high thickness. In an uncontrolled natural drying process, perovskite precursor often undergoes a low supersaturation degree and then comes to the nucleation with fewer nuclei. Accomplished with the preferential growth sequentially, the final morphology exhibits a dendritic structure with poor coverage and a short-circuit path.[4,52] According to classical nucleation theory, nucleation is the process where the nuclei (seeds) act as templates for crystal growth, where the crystal's total free energy is defined as the sum of surface and bulk free energy $\Delta G = 4\pi r^2\gamma + 4\pi r^3 \Delta G_v$, where $\Delta G_v = -k_B T \ln(S)/v$, where T represents the temperature, k_B represents Boltzmann's constant, S is the supersaturation of the solution and v is the molar volume. (**Figure 3a**).[52,59] The LaMer mechanism, which conceptually separates nucleation and growth into two parts, where the nucleation rate V_1 and growth rate V_2 highly depend on the crystal's total free-energy ΔG and the supersaturation S (Figure 3b,c).[52,59,60] The crucial point for homogenous films is to increase the nuclei numbers and relatively slow down the growth process, which could be realized by supersaturation control through the manageable removal of host solvents and the assistance of chemical additives. Physical procedures including the anti-solvent approach, gas quench, vacuum-assisted drying, and hot-casting methods can rapidly remove the host solvents and promote supersaturation to a high degree while the chemical approaches including solvent

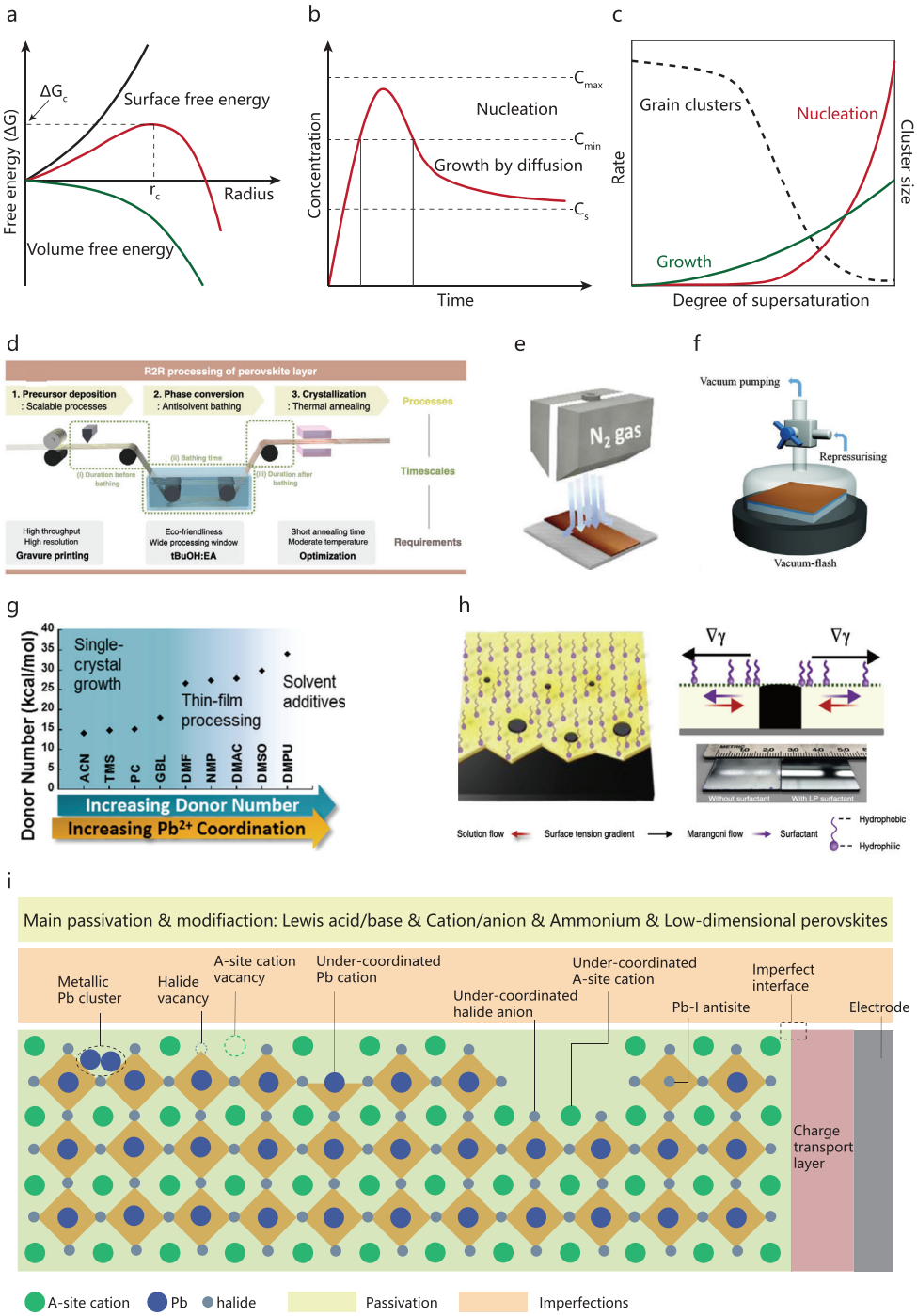

Figure 3. Strategies to improve PCEs of PSMs, including crystallization control and defect management. a) Free energy diagram for nucleation. b) LaMer diagram schematic, which divides nucleation and growth processes into three stages. c) The nucleation and growth rates as a function of the supersaturation degree, and the corresponding grain-cluster size. d) Schematic illustration of an anti-R2R solvent bath approach process. Reproduced under the terms of the CC-BY Creative Commons Attribution 4.0 International License (http://creativecommons.org/licenses/by/4.0/).[65] Copyright 2020, The Authors, published by Springer Nature. e) Schematic illustration of a gas-quench process equipped with a nitrogen knife. Reproduced with permission.[62] Copyright 2018, Elsevier B.V. f) Schematic illustration of the vacuum-assisted drying process. Reproduced with permission.[63] Copyright 2016, The American Association for the Advancement of Science. g) Donor number with respect to different types of solvents. Reproduced under the terms of the Creative Commons CC BY-NC 4.0 License (https://pubs.acs.org/page/policy/authorchoice_termsofuse.html),[72] Copyright 2017, The Authors, published by American Chemical Society. h) Schematic illustration for the suppressed solution flow dynamics in the presence of surfactant. ∇_γ, denotes the surface tension gradient. The insert is a photographic image of blade-coated perovskite films without and with LP surfactant. Reproduced with permission.[40] Copyright 2018, The Authors, published by Springer Nature. i) Imperfections in perovskite solar devices and their corresponding passivation strategies.

engineering, additive approach, and compositional engineering are often utilized to form intermediate phase to retard the crystallization process.[4,58–65]

5.2.1. Physical Approaches

The anti-solvent dripping is widely used at the cell level for morphology control while the anti-solvent bath is proposed in modules for the fast removal of the host solvents (Figure 3d). Based on this strategy, a Roll-to-roll (R2R)-processed flexible perovskite PV device through gravure printing was realized at a pilot scale.[65] When applying this method in industrial manufacture, the large consumption of the anti-solvent could become a concern. After multiple extractions, the anti-solvents will be contaminated or diluted, which demands the necessity of large storage quantities or efficient purification systems at extra costs. In addition to the methods, gas-quench methods where a forced gas flow is produced by a so-called gas knife to expedite solvent removal are commonly used (Figure 3e).[62] From an industrial perspective, this method has the greatest potential due to the ease of scale-up and feasible integration with the existing technology. Vacuum-assisted drying methods are also suitable for scale-up because the requirements can be readily reached in the mature vacuum industry (Figure 3f).[63] One concern here is the vacuum environment to accelerate solvent evaporation can be applied only after the film coating completes, which proposes stricter demands, for example, an expanded deposition window to enable the film homogeneity. Hot-casting methods, where the perovskite precursor is deposited on a pre-heated substrate enable ultrafast production and high throughput.[64,66,67] Pre-heated substrates facilitate solvent removal and sometimes ameliorate the wettability of the substrates, reducing the surface energy and nucleation energy. Typically, as-deposited wet perovskite films require post-thermal treatments to remove solvent residue, while hot-casting can sometimes eliminate this process, significantly saving fabrication time in manufacturing.[4,5,40,66,67] In addition, Angmo et al. further proved that the hot-deposition method was essentially independent of humidity level and demonstrated improved stability and reproducibility compared to anti-solvent methods, suitable for large-scale manufacturing in the ambient environment.[67]

5.2.2. Chemical Approaches

When the degree of supersaturation is too high, it leads to a strong nucleation burst, resulting in undesirable small grains. Additives play the role of regulating the nucleation and growth process, especially retarding the crystallization process to a moderate rate. Chloride-based compounds (e.g., MACl and $PbCl_2$) resulted in smoother films and certified PCEs exceeding 25% due to the formation of a chloride-containing intermediate phase.[38,68] Systematic investigations of other additives like acid and alkaline were also reported.[69,70] The acid or alkaline additions were found to coordinate with the precursor and adjust the pH value of the solution, which affected the colloid states and crystallization kinetics. A bunch of additions obeying the similar crystallization mechanism called "Lewis acid-base adduct theory" have excellent morphology regulation.[71–73] Lead halides are regarded as strong Lewis acids with empty orbital that are ready to form adducts with Lewis bases with lone electron pairs. The formation of the acid-base adduct has a higher reaction energy barrier and solubility than its monomers, slowing down the nucleation and growth rates. For example, solvents like dimethyl sulfoxide (DMSO) and *N*-methyl pyrrolidone (NMP) with increased donor number have a good coordinating ability with Pb^{2+} and are commonly used to control morphology and expand the processing windows (Figure 3g), highly promoting the film reproducibility.[72]

The ink surface tension affects the contact angle of the precursor with the surface, and the surfactant additives were used to modify the adhesion of perovskite ink on hydrophobic substrates and to alter the crystal growth process.[40] Surfactants could decrease the surface energy of the substrate and reduce the heterogeneous nucleation energy of the perovskite, facilitating homogeneous nucleation and more dense films. For example, the surfactant additives of ≈20 ppm precursor can significantly improve the blade-coating quality of perovskite films on hydrophobic PTAA at a high coating speed of 180 m h^{-1} and boost stabilized mini-module PCEs to 15.3% and 14.6% at designated areas of 33.0 and 57.2 cm^2, respectively (Figure 3h).[40]

5.3. Defect Management of the Device

Intrinsically, low defect formation energies in perovskite crystals make defects easily form with layer deposition. Perovskite contains different types of point defects, including but not limited to vacancy, interstitial, anti-site substitution, Frenkel defect (interstitial and vacancy created from the same ion), Schottky defect (anion and cation vacancies occurring together), and substitutional impurity.[73–77] Defects act as non-radiative recombination centers and serve as the channel for ion migration, leading to a large open-circuit votage (V_{oc}) deficit and poor performance. Various agents aiming at passivating defect-surplus regions (grain boundaries and surface) have been developed, including inorganic metallic salts, low-dimensional wide-bandgap perovskites, organic small molecules or polymers, and ionic liquids (Figure 3i).[75–77] For example, some non-volatile organic Lewis bases with lone electron pairs will effectively passivate the uncoordinated Pb^{2+} defects while the Lewis acids aim at the uncoordinated halide defects both by forming Lewis adducts.[75] In addition, defects can be easily generated on the top or bottom of a given layer during the interface formation with other layers' deposition. For example, commonly used electron transporting materials C_{60} could induce additional trap states when deposited on perovskites, leading to a reduced quasi-Fermi level splitting.[78] Interface modification could inhibit defect formation, rearrange energy alignment, modify carrier selectivity, and enhance carrier extraction.[78–80] For instance, the inorganic insulator lithium fluoride (LiF) and magnesium fluoride (MgF_2) were proven as good interfacial modifiers between perovskite and electron transporting layer (ETL), which was effective at reducing the non-radiative recombination loss and facilitating the extraction of electrons by the formation of a surface dipole.[19,78,80] Here, we just provide a brief summary, and detailed reviews about defect passivation can be found elsewhere.[75]

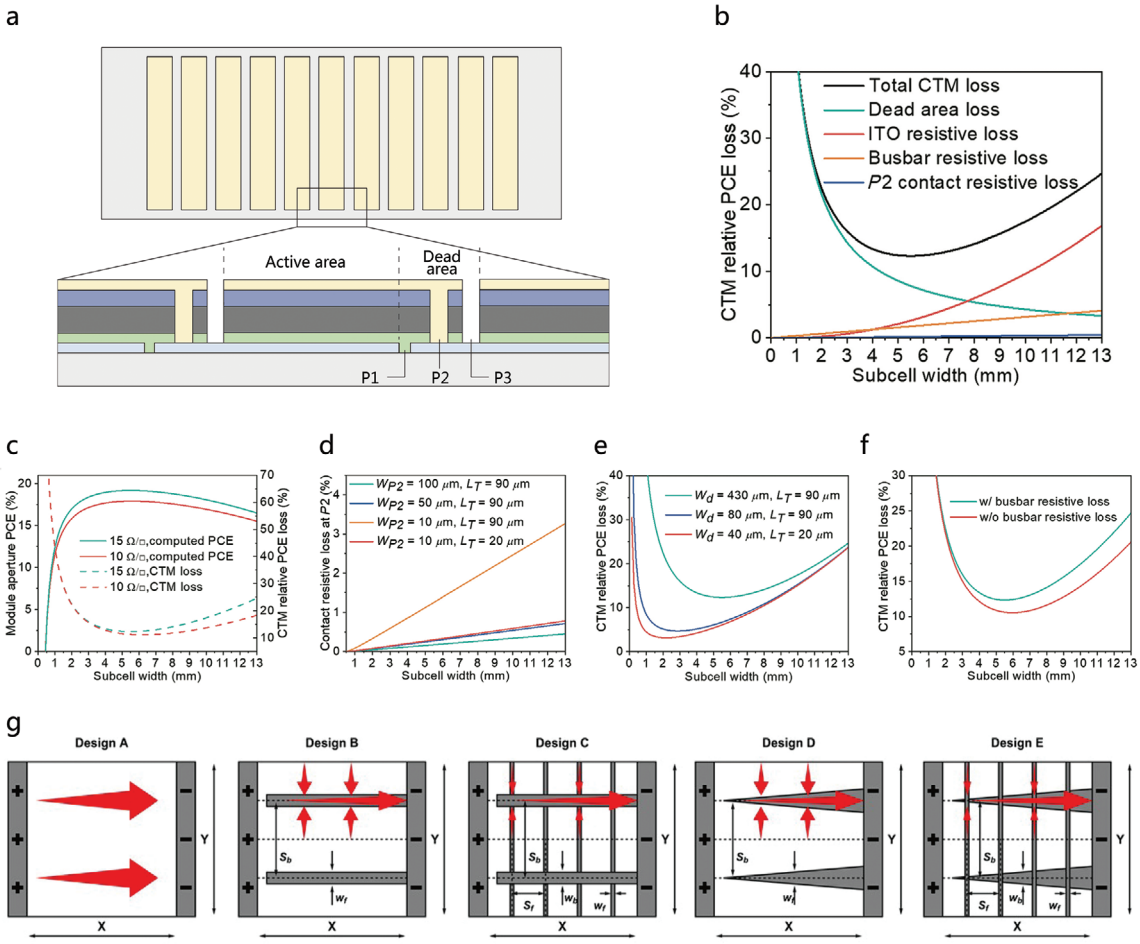

Figure 4. Module design for improved module performance. a) Schematic illustration of a series-connected perovskite module. b) The modeled impact of the module-scribing geometry on the total CTM loss in a series connection. c) Impact of ITO sheet resistance on CTM loss and module PCE. d) Impact of P2 width and transfer length of metal-ITO to the contact resistive loss at P2. e) Impact of dead area width (W_d) on CTM loss. f) Impact of busbar resistance on module PCE. b–f) Reproduced under the terms of the CC BY Creative Commons Attribution 4.0 International License (http://creativecommons.org/licenses/by/4.0/).[50] Copyright 2022, The Authors, published by the American Physical Society. g) Five modeled cell designs: design A: a cell without a metal grid, design B: a cell with a metal grid consisting of parallel metal busbars, design C: a cell with a metal grid composed of parallel metal busbars and fingers, design D: the same as for design B but with busbars that taper in width, design E: the same as for design C but with busbars that taper in width. Reproduced with permission.[83] Copyright 2018, John Wiley & Sons, Ltd.

5.4. Optimal Design of Perovskite Modules

5.4.1. Total Power Loss of Perovskite Modules

From geometric consideration, a high GFF is essentially important to enhance the module utilization ratio.[50,81] Reduction of the dead area width is always desired but is limited by the current scribing technology. Another way for a larger GFF is to improve the sub-cell width but the resultant width increase of active area could bring additional resistive loss. Therefore, balancing the losses caused by resistance and the dead area is essential for maximizing module PCE and parameters including sub-cell width, scribing width, and electrode designs need to be precisely optimized (**Figure** 4a–f).[50] In a PSM, the P1, P2, and P3 scribes are critical to forming an ideal series connection. The P1 scribe is used to separate the TCO electrodes, the P2 scribe provides connections between the top contact of one cell and the bottom contact of the next cell, and the P3 scribe divides the top contact between adjacent cells (Figure 4a).

The total cell-to-module (CTM) power loss is composed of four parts: geometrical loss due to the existence of dead area (f_G), active-area ohmic loss due to the TCO resistance (f_{TCO}), interconnection ohmic loss related to P2 step (f_{P2}) and busbar ohmic loss (f_B). By taking the parameters in Table S5 (Supporting Information) for calculation, the corresponding total loss versus the sub-cell width is shown in Figure 4b, where a minimum loss of 12.3% is reached at a sub-cell width of 5.5 mm.[50]

5.4.2. TCO Substrates and Novel Electrode Designs

The resistive loss of active area can be further mitigated by the substitution of high-conductivity TCO but at a sacrifice of light harvest. The computed CTM losses and module

efficiencies based on 10 and 15 Ω $\square^{-1}$ ITO are plotted according to the extracted parameters from practically fabricated PSCs. As shown in Figure 4c, although the 10 Ω $\square^{-1}$ ITO-based device delivers a minor CTM loss, the decreased small-cell PCE results in a lower module PCE, mainly resulting from the optical loss due to thicker ITO. In this case, 15 Ω $\square^{-1}$ ITO should be chosen due to a more significant influence of light transmission loss than transport loss.

The busbar resistive loss cannot be ignored when the sub-cell current is significant or when the conductivity of the busbar is insufficient (Figure 4f). Strategies such as applying thick metal ribbons and adopting novel designs like series and parallel connections have been developed to minimize such loss.[50,82] Wilkinson et al. systematically modeled various front metal grid designs (Figure 4g) to determine the efficiency limits of each case.[83] For the cells with an area exceeding 200 cm^2, higher PCEs were demonstrated from the design with parallel metal grids, like designs C and E, but at the expense of increased complexity. The use of tapered bars in designs D and E provided a performance improvement for highly resistive cells, thus, further optimization of metal grid thickness and dimensions reveals a possible PCE enhancement by the balanced resistance and parasitic absorption.

5.4.3. Line Scribing and Safety Areas

As mentioned above, larger GFF demands a negligible dead area that the P1, P2, and P3 lines, and the gaps between the lines (safety areas), have to be as narrow as possible. P1 and P3 lines are used to separate the electrodes of adjacent cells electrically and a width of 15 µm for both was considered sufficient to provide insulation.[50,82] The P2 scribe plays the role of connecting the adjacent sub-cells and needs to be sufficiently optimized for the minimum resistive loss. The contact resistance at P2 is related to the line width and contact resistivity between the electrode and TCO, where a larger width and smaller resistivity are essentially desired. To minimize the resistivity, TCO damage, residues left by incomplete removal, or the redeposition of debris should be avoided. The minimum P2 width is tightly related to the resistivity and is reflected in the parameter called transfer length (L_T), which refers to the length that the charges travel in the TCO before they are transferred to the contact. When the P2 width reaches a comparable value with L_T, the contact resistance can be ignored (Figure 4d). Besides, to avoid the possible overlapping between sub-cells, it is essential to introduce a safety area between P1-P2 and P2-P3. These areas are supposed to be narrow enough to achieve high GFF but also protect adjacent sub-cells from being shorted. Previous literature has set the safety areas of P1-P2 and P2-P3 to 50 µm each without compromising the module performance[84–88] Dai et al. believe a total dead area without safety areas is achievable, which can dramatically reduce the total CTM loss to only 4.7% (Figure 4e).[50]

6. Some Considerations in Industrial Production

In industrial production, several technical considerations must be taken into account. The first is the production output which is reflected in tact time. Assuming a 100-MW production line with a module size of 1.2 × 0.6 m, the tact time is calculated to be ≈30 s per piece when setting the total-area PCE at 18% (20 h day^{-1} and 330 days $year^{-1}$). Admittedly, increasing the amount of production line will reduce the tact time but at the expense of higher investment costs.

The deposition of perovskite films is a time-consuming procedure by both solution and vacuum approaches. The use of volatile solvents can enable a rapid drying of deposited perovskite film and therefore a high processing speed in solution approaches, but volatile solvents such as acetonitrile usually perform better in methylammonium (MA)-rich systems, which are not promising candidates toward commercialization.[5,89–91] Another time-consuming procedure is the annealing process for both perovskite and CTLs, which usually takes several minutes. Irradiation like near-IR radiation or pulsed light has been proven efficient in the annealing-time reduction.[91,92] In addition, a spray rapid spray plasma processing (RSPP) was proposed to overcome this time limitation by crystallizing the perovskite film through thermal and plasma energy. This RSPP method not only omits the post-annealing process but also reduces the deposition time as it does not require any start-up time before producing uniform coatings, demonstrating a processing speed of 12 m min^{-1} but a slightly lower PCE of 18% at the cell level.[93] Recently, a co-deposition method that forms HTLs and perovskite films together simplifies the manufacturing processes and lowers the barriers to commercialization.[94]

The reproducibility in the industry is crucial because it is the guarantee of the qualification and the yield rate. It sets requirements for raw materials, precursor composition, processing, etc. For example, the precursor is supposed to be stable for a period of storage time or at least unchanged during the deposition periods before its exhaustion, and the processing window for fabrication should be expanded to achieve a homogeneous film. Usually, PSCs fabricated using fresh precursor solutions exhibit good PCEs, but after storage for a few days, the precursors no longer produce high-efficiency devices due to the oxidation of I^- ions to I_2.[61] A low-cost reductant, benzylhydrazine hydrochloride (BHC) can reduce I_2 to I^- and thus, restore degraded precursor solutions and improve fabrication reproducibility.[61] Besides, due to the limited solubility of lead halide, the commonly used solvent mixture for efficient PSMs is 2-methoxy ethanol (2-Me) and DMSO, which easily lead to precipitation after several hours or even tens of minutes. Solvent engineering or additive engineering will be conducive to the precursor stability enhancement and the processing window expansion.[4,5,40,41,61] Finally, some characterization techniques like photoemission spectroscopy need to perform real-time monitoring during fabrication for the minimization of the sequential loss.[4,5,95] More investigations are supposed to be devoted to guaranteeing the smooth manufacturing of PSMs.

7. The Stability Issues and Corresponding Solutions

7.1. The Stability Evaluation Protocols

As noted above, the standard IEC 61215is set for the evaluation of the degradation of silicon panels which contains several accelerated tests performed at damp-heat, UV, and thermal-cycle

conditions.[17] Some regulations in the IEC standard are not applicable to perovskites due to their peculiarities. The ISOS protocols, providing standardized aging experiments to evaluate the stability of organic photovoltaics (OPVs) first, were recently extended to set specific stability rules for perovskite PVs.[18] Unlike IEC qualification standards, a perovskite PV device cannot pass or fail ISOS standards because these protocols are only intended to provide an aging framework for more comparable results.[18,96,97] Accelerated aging tests from these protocols expedite the degradation but do not provide direct information on solar cells' expected lifetime under actual operational conditions. In other words, the complete pass of IEC 61215 does not guarantee a 20-year lifetime of perovskite PV devices.[11,16] The concept of acceleration factor (AF) has been proposed to correlate the real-world lifetime to that obtained under accelerated stress.[18,98] AF of PSCs for each stress could be derived from a physical model and has yet to be unified to date. At this moment, we encourage researchers in the PV community to adopt the above two stability protocols before a more suitable protocol comes to reach a consensus.

7.2. Instability from the Individual Layers (perovskite, CTLs, electrode) and the Interfaces

A summary of instability issues appearing from the layers and interface is illustrated in **Figure 5** as a comprehensive reference. The instability of the perovskite mainly originates from its soft-lattice nature, undesired phase transition, and defect-mediated ionic migration, where the last can be triggered or intensified by external humidity, heat, illumination, electrical field, and internal lattice strain (Figure 5a). The ionic nature and hygroscopic character of ammonium salt render perovskites easy to damage when exposed to humidity, weakening the interaction between the cation and the PbI_6 and allowing for faster deprotonation of organic cations.[99,100] Thermal instability mainly originates from relatively weak bonding between the organic components and PbI_6 because formamidinium (FA^+) with an enhanced number of hydrogen bonds is found to be more stable than MA^+ under thermal stress.[99,100,102] In addition, the residual lattice strain usually due to the CTE mismatch between perovskite and substrates could result in accelerated degradation because it lowers defect formation energy and activation energy for ion migration.[101] δ-phase formamidinium lead iodide ($FAPbI_3$) perovskite has lower free energy than the α-phase at room temperature, thus the metastable α-$FAPbI_3$ with higher free energy tends to transform into the δ-$FAPbI_3$ with photo-inactive properties spontaneously (Figure 5b).[102] Under illumination, excess photocarriers provide the potential for chemical reactions such as free radical formation and iodide ion oxidization, which results in the coupled formation of neutral iodine interstitials and iodide vacancies, further leading to metallic lead formation and irreversible decomposition. The detrimental ion migration will lead to several anomalous phenomena such as light-induced halide segregation (Hoke effect) and cation segregation, that could cause irreversible performance decay (Figure 5a).[99,100,102] In short, degradation pathways are related to the nature of perovskites but defects would significantly accelerate these processes because they could be the starting point of the degradation.

Some CTLs are intrinsically unstable or cause reactions at the interface. For instance, inorganic n-type semiconductor zinc oxide (ZnO) was reported to react with perovskites during thermal annealing andTiO_2 could lead to UV-light instability at the TiO_2/perovskite interface.[99,103] The most efficient HTM Spiro-OMeTAD also faces severe stability issues arising from its low glass transition temperature and doping.[99,104] The above-mentioned ion migration (especially for halide) not only happens in perovskite but also easily transports through the interface, and finally reaches the metal electrode, leading to the halide deficit and electrode corrosion (Figure 5a).[99,104] Conversely, even the most stable metals, like platinum, can diffuse and react with halide species in the perovskites under heat or illumination.[99] Besides, metal contacts could also form a redox coupled with Pb^{2+} in perovskite films. Non-passive metals, like alumina (Al), can rapidly reduce Pb^{2+} to Pb^0 and decompose perovskites.[99,105,106]

The key point to solve this kind of instability is to isolate or relieve the external stress, enhance the internal bonding, and mitigate the ion migration. First of all, encapsulation is a feasible way to prevent the oxygen and humidity of the device (**Figure 6a**).[107] Ethylene-vinyl acetate (EVA), typically used in c-Si modules, is not applicable here due to its high water vapor transmission rate (WVTR) of exceeding 20 g m^{-2} d^{-1} and high processing temperature (>140 °C).[108] Polyolefin (POE) with a lower laminating temperature of 120 °C along with butyl rubber, a kind of synthetic rubber with good air and water tightness, is widely used in the PSM encapsulation considering their multiple advantages like low WVTR and high insulation.[109,110] Second, to reduce the negative effects arising from the thermal, a combination with a cooling system like radiative cooling, heat pipe, and interfacial evaporation can be considered in a cost-effective way (Figure 6b).[111,112] Finally, multiple approaches for inhibiting phase transition and mitigating the ion migration either in the film or across the interface have been developed, including compositional engineering, bulk/surface defect passivation, crystallinity, orientation control, morphological improvements, interface modification, diffusion barrier construction, etc.[4,102,103,113–116] The overall guide can be explained by decreasing the free energy of desired products and increasing the energy barrier of undesired reactions (Figure 5b). For example, the α-$FAPbI_3$ could be stabilized at room temperature by surface-free-energy tunability, such as the incorporation of bulker cations expelling at the grain boundaries and surface or the volume reduction to nano size.[99,116] In addition to the removal of the migration channel like defect passivation, the ion migration can be also mitigated by increasing the energy barrier for mobile ions through the steric and electrostatic interactions, such as A-site cation doping (e.g., potassium ions, (K^+)). These discussions are covered in previous comprehensive reviews and will not be elaborated thoroughly here.[116]

7.3. Accelerated Degradation at the Interconnection

Some other instability issues specific to modules like damages from reverse bias, accelerated degradation at interconnection, potential induced degradation (PID), and so on, should also raise the researchers' attention in the perovskite community (Figure 5c–g), parts of which have been investigated for c-Si technologies already.[3,4,96,117–120]

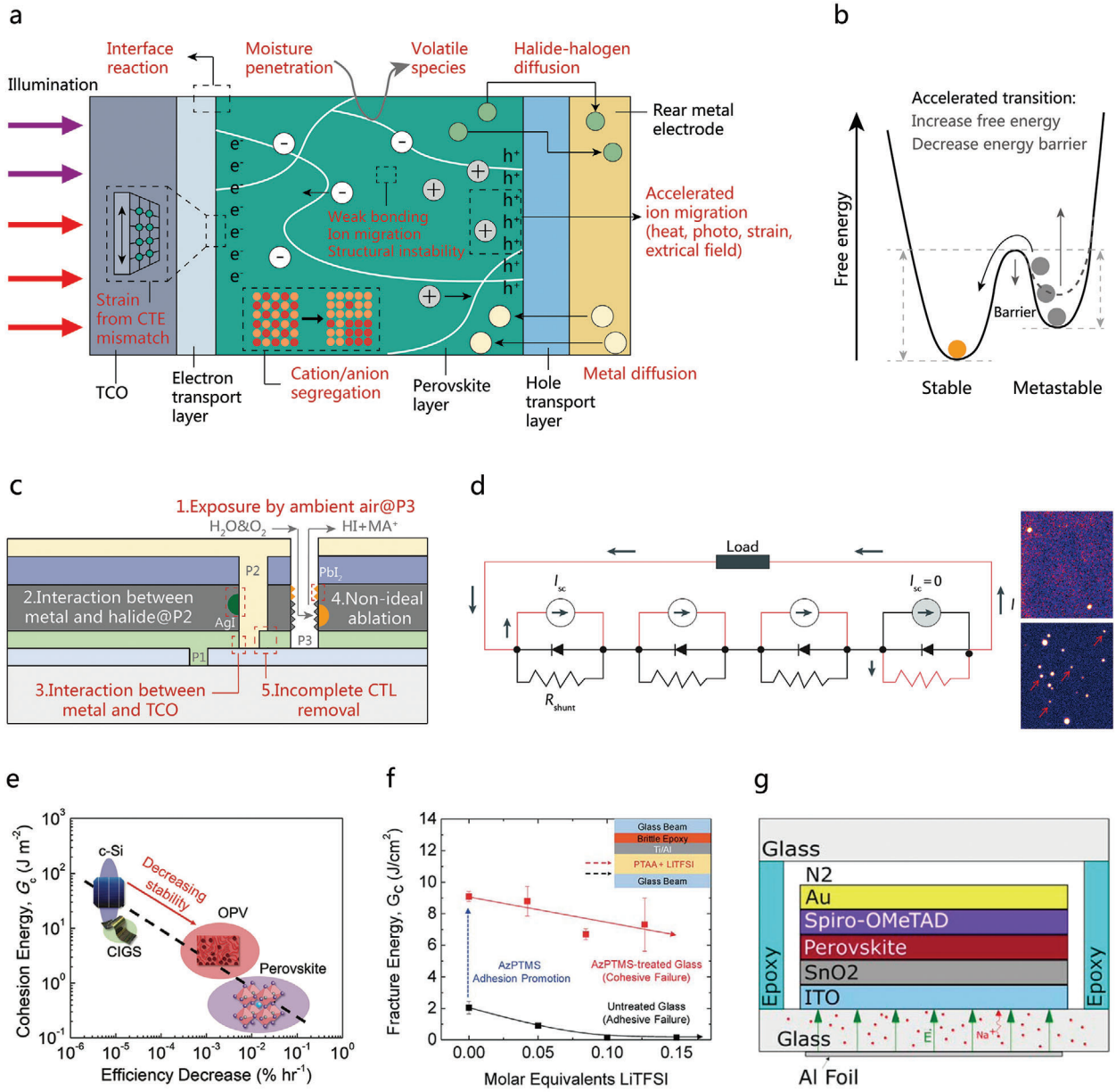

Figure 5. Instability issues of perovskite solar devices at the cell and module levels. a) Illustration of instability issues at the cell level. b) Illustration of free energy relationship between stable and meta-stable phase at room temperature. c–f). Illustration of instability issues at the module level. c) Fast decomposition at the interconnection. d) Partial shading of the module causes reverse bias, shunting failure, and hot spot formation in the shaded sub-cells. Reproduced with permission.[4] Copyright 2018, Macmillan Publishers Limited. Reproduced with permission.[47] Copyright 2020, Royal Society of Chemistry. e) The measured cohesion energy and degradation rate as a function of solar cell active material, showing a correlation between mechanical integrity and long-term reliability. Reproduced with permission.[122] Copyright 2017, WILEY-VCH Verlag GmbH & Co. KGaA, Weinheim. f) Influence of LiTFSI concentration on fracture energy and pathway of PTAA deposited on glass beams with/without 3-azidopropyltrimethoxysilane (AzPTMS) adhesion promotion. Reproduced with permission.[123] Copyright 2017, Royal Society of Chemistry. g) An encapsulated n-i-p perovskite solar cell was used in the PID experiment. The high voltage was applied between the short-circuited solar cell and the Al foil attached to the substrate. Reproduced with permission.[126] Copyright 2019, WILEY-VCH Verlag GmbH & Co. KGaA, Weinheim.

First, the P3 scribing leaves an opening in the module, which makes it easy for moisture and oxygen to penetrate for reaction (Figure 5c).[4,120] Second, the P2 scribing leads to the direct contact of metal with perovskites, where halide species easily diffuse into or directly react with the metal electrode.[99] Third, the P2 scribing also leads to the direct contact of metal with the bottom TCO electrode, where reactions like the oxidation of metal (e.g., Al on ITO) will happen, increasing resistive losses at the interconnection.[4] Fourth, the non-optimized laser settings can lead to the partial decomposition of perovskites during the scribing process, with the formation of a small amount of lead iodide (PbI_2) at the edges and accelerated decomposition. Finally, the

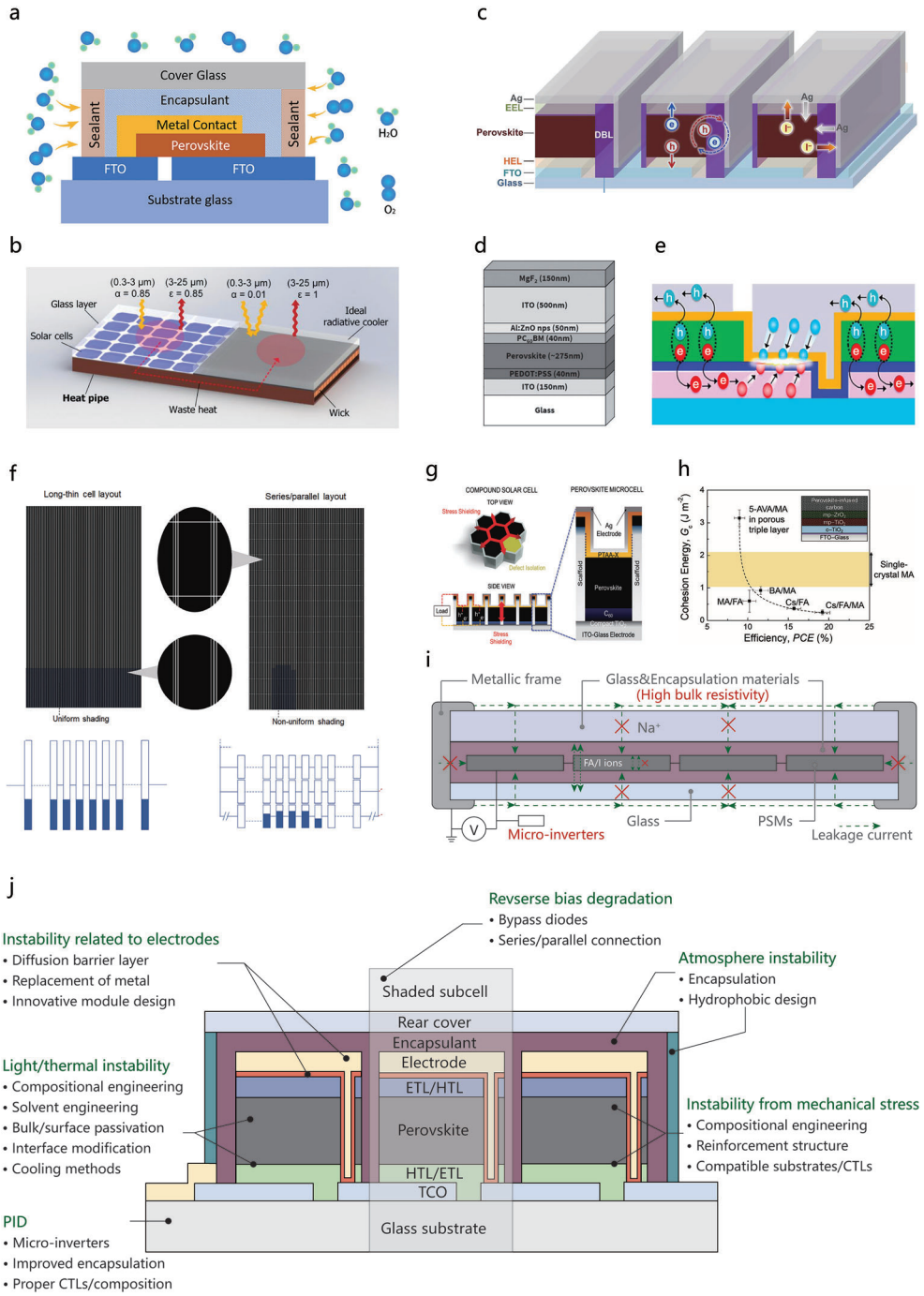

Figure 6. Strategies used for the stability improvement of PSMs. a) Illustration of the encapsulation of PSMs. Reproduced under the terms of the CC BY-NC-ND 4.0 Attribution-NonCommercial-NoDerivs 4.0 International license (https://creativecommons.org/licenses/by-nc-nd/4.0/).[107] Copyright 2022, The Authors, published by American Chemical Society. b) A cooling system for PVs combining heat pipe and radiative cooling. Reproduced with permission.[111] Copyright 2021, Elsevier Ltd. c) Illustration of the diffusion barrier constructed in the PSM (EEL is the electron extraction layer and HEL is the hole extraction layer). Reproduced with permission.[113] Copyright 2019, Elsevier Inc. d) A PSC employing a transparent TCO electrode. Reproduced with permission.[114] Copyright 2016 WILEY-VCH Verlag GmbH & Co. KGaA, Weinheim. e) The conceptual module structure, consisting of patternless CTLs and patterned photoactive layer. Reproduced under the terms of the CC BY Creative Commons Attribution 4.0 International License (http://creativecommons.org/licenses/by/4.0/).[115] Copyright 2016, The Authors, published by Springer Nature. f) Schematic of vertical long-thin cell layout, the schematic of series/parallel cell layout by including one extra scribe, and their equivalent circuit of the solar modules. Reproduced with permission.[118] Copyright 2022, Elsevier Inc. g) The top and side view of the scaffold PSCs and a single perovskite microcell. Reproduced with permission.[124] Copyright 2017, Royal Society of Chemistry. h) The measured average G_c and PCE values as a function of cation composition, show a trade-off between reliability and efficiency. Reproduced with permission.[122] Copyright 2017, WILEY-VCH Verlag GmbH & Co. KGaA, Weinheim. i) Schematic illustration of several possible leakage current paths in PID condition. j) Summarized strategies used for the stability improvement of PSMs.

incomplete removal of the CTLs at the interconnection will bring in increased resistance between the adjacent electrodes.[86,90]

To protect the module from moisture and oxygen penetration at P3, one effective way is to adopt an encapsulation described in Figure 6a.[107] However, the encapsulation strategies at the module level are somehow different from that at the cell level, because all stackings are in contact with encapsulation material at the P3 area. Therefore often, the encapsulation strategy developed for individual cells should be re-optimized and more inert for the modules. To prevent ion diffusion and possible reaction between metals and perovskite, a diffusion barrier layer between the electrode and CTLs and the replacement of metal electrodes with other inert materials like carbon pastes or TCO electrodes are valid approaches (Figure 6c,d).[113,114] Another promising approach to avoiding the contact of perovskite and the metal electrode is based on an innovative module structure originally used for OPVs (Figure 6e).[115] In this structure, only the perovskite layer is patterned and the carrier recombination occurs at the interface between HTL and ETL. This approach not only prevents the direct contact of perovskite with a metal electrode but also simplifies the manufacturing process. Finally, the non-ideal ablation and incomplete CTL removal can be optimized by tuning the laser parameters, like time duration, wavelength, and incident direction, as mentioned above, improving PSMs' efficiency and stability.[86,87]

7.4. Damages from Reverse Bias

The performance of the module is imposed by the individual subcell showing the lowest electrical performance. Typically, when one or more sub-cells are shaded in a series connection, the shaded cells do not generate current but are subject to a high reverse bias, which could lead to inverted-bias junction damage and the formation of a local hot spot (Figure 5d).[4,47,118] These degradations are strongly related to spatial inhomogeneity and electric field-induced ion migration. The investigation and improvement of the device stability under reverse bias are crucially necessary for real-world applications.

One potential solution to solve the reverse bias degradation in PSMs is using bypass diodes, whose validity has been already proven in c-Si (Figure S5, Supporting Information). The typical reverse bias breakdown voltage for PSCs ranges between −1 and -4 V, vastly lower than that of c-Si counterparts (−15 V).[89,109] The maximum number of solar cells per bypass diode that can be used while maintaining the diodes working is $N_{max} = (V_{to} - V_{br})/V_{oc} + 1$, where V_{br} is the reverse breakdown voltage, V_{oc} is the open-circuit voltage and V_{to} is bypass diode turn-on voltage and typically 0.6 V for a Schottky diode.[117] Thus, the low reverse breakdown voltage requires bypass diodes five to ten times as much as silicon to ensure the same level of protection. Recently, another solution from module design has been proposed to solve the irreversible damage from partial shading, where the series/parallel connection of cells is utilized in a module (Figure 6f).[118] This strategy is simple and only requires one additional laser step, converting what was originally a single string of serially connected cells into a parallel connection of many strings. In this case, the partially shaded cell string would operate at, or near, an open circuit because the unshaded strings provide the parallel electrical connection, minimizing the chance of reverse-bias heating.

7.5. Instability from Mechanical Stress

In commercial c-Si modules, delamination often occurs between the encapsulating polymer and cells. It causes an increase in light reflection and moisture penetration inside.[120] Mechanical stresses like hail or wind, loading, temperature recycling, and the residual strain, for example, from CTE mismatch (CTE: $\approx 45 \times 10^{-6}$ K^{-1} of perovskite versus $\approx 10 \times 10^{-6}$ K^{-1} of glass), can magnify the influence of brittle nature and weak layer bonding, causing delamination or fracture in stacking layers of PSMs.[99,120] This decline not only leads to a loss of ohmic contact but also creates an accelerated pathway for the diffusion of volatile compounds. The "critical" adhesion or cohesion energy G_c (J m^{-1}), defined as the energy needed to cause delamination between layers or failure in a layer, is used to measure mechanical integrity.[122,123] In PSMs, when layers are weakly bonded with poor adhesion, the delamination will first occur before the cohesion fracture happens (Figure 5e,f). With improved adhesion, the fracture starts from the weakest layers first, usually, the CTLs in a completed device. The typical cohesion fracture energy of perovskite, [6,6]-phenyl-C_{61}-butyric acid methyl ester (PCBM), and PTAA is 0.5, 0.1, and 0.17 J m^{-2}.[99,122–124] Although the G_c of perovskite is the highest among all the stacks, it is still significantly lower than OPVs (≈5–15 J m^{-2}), CIGS (≈10 J m^{-2}), and c-Si (≈10–200 J m^{-2}) (Figure 5e).

The brittle nature and weak layer bonding can cause delamination or fracture, especially for devices with residual strain and under external stresses.[99] To improve mechanical stability, the first strategy is to minimize the CTE mismatch and release the lattice tension, for example, using substrates with CTE similar to that of the perovskites. Another strategy is to improve the adhesion or cohesion energy G_c, including tuning perovskite composition, controlling the morphology and roughness, employing a mesoporous or reinforced scaffold structure (Figure 6g), and selecting suitable CTLs along with encapsulation materials. For example, the G_c of perovskites was found to be increased with the enlarged grain size (from <500 nm to >10 μm) and the incorporation of bulker cations like butylammonium (BA^+) (Figure 6h).[122]

7.6. PID

In a solar plant, individual modules are often connected in series to increase the voltage of the system, reaching a potential difference of several hundred volts.[96,99,120] The metallic structures of modules are commonly grounded for protection against electrical shocks. Due to this high electrical voltage between modules and the ground, current leakage is possibly formed between PV modules and the grounded framework when the insulation is not perfect, which results in a decrease in shunt resistance. In n-type c-silicon modules, the negative charges were found trapped within the anti-reflection layers (silicon oxide/silicon nitride (SiO_x/SiN_x)) due to their high resistivity.[96] The accumulated charges increase surface recombination and reduce the PV parameters. One main cause of PID results from the migration

of alkaline metal ions, such as sodium ions (Na^+) in substrates, through the encapsulation materials and toward the solar cell under the high electric field (Figures 5g, 6i).[95,120,125,126] In addition, when moisture penetrates the module, a combination of Na^+ reduction and moisture ingress will result in non-reversible electrochemical corrosion of the TCO.[95,120,125,126] When switching to perovskites, the PID can also adversely affect the stability mainly due to the increased ionic migration and defect formation, resulting in severe current leakage and improved recombination. According to the standard IEC 62804-1, the PID experiment was conducted using the foil method with a high voltage of 1000 V for 18 h, whereas the perovskite device was stored in an environmental chamber at 60 °C and less than 60% relative humidity (Figure 5g). Previous reports showed that PSCs were extremely susceptible to PID tests, showing a performance degradation of up to 95%.[125,126]

In c-Si modules, the PID can be mitigated by the modification of anti-reflection (AR) coating, insertion of an interlayer between the Si and the AR coating, and the adoption of micro-inverters for an opposite potential, some of which can be transferred to PSMs.[96] Because PID in PSMs not only results from the ion migration in the glass substrates but also in perovskites, suppressing ion migration, especially in perovskite becomes significantly crucial. Choosing suitable perovskite composition and CTLs, employing suitable encapsulation materials or/and glass sheets with high bulk resistivity, and adopting micro-inverters to tune potential will be a future research direction (Figure 6i). For example, PSCs using a PCBM layer (although thermally unstable) as ETL have demonstrated good stability under high electrical fields, only showing a 4% degradation after an 18 h standard PID test.[125,126] The encapsulation material with high bulk resistivity and low WVTR, like POE is supposed to effectively hold out against PID, aiming at either reducing the current leakage or preventing the moisture from penetrating for reactions. For commercialization, more investigation on the full recoverability after PID damage, and deteriorated mechanisms and kinetics of PID in perovskite devices should be applied.[126] A comprehensive summary of corresponding solutions to instability issues at the module level, either externally or internally is plotted in Figure 6j, providing a straightforward understanding for readers. Commonly, a combination of several strategies described in Figure 6j is selected, which opens up the effective path toward stability enhancement. For example, a holistic interface stabilization strategy by modifying all the layers and interfaces, including the perovskite layer, charge transporting layers, and device encapsulation was employed to improve the efficiency and stability of PSMs.[106]

8. Cost Analysis and Life Cycle Assessment (LCA)

8.1. Cost Analysis

At this stage, it is difficult to precisely evaluate the actual manufacturing cost of PSMs because it is tightly related to multiple uncertain aspects: configuration selection, raw materials, fabrication processing, factory location, labor wages, etc. Even for an approximate evaluation, several assumptions, which might be partially overthrown in the future, are needed. Here, we review some cost analysis of different PSM types and discuss how the manufacturing cost can be affected by the above considerations.[4,127–130] In addition, cost models rely on a lot of assumptions and can show a range of LCOEs. Readers should critically evaluate these techno-economic assessments.

In an early analysis, Cai et al. proposed the cost calculations of two types of perovskite modules: module A with a structure of FTO/(TiO_2/ZrO_2/carbon)/perovskite (ZrO_2 refers to zirconium oxide) and Module B with a structure of ITO /(poly(3,4-ethylenedioxythiophene)):(poly(4-styrenesulfonate))(PEDOT:PSS)/perovskite/PCBM/calcium (Ca)/Al. The cost is divided into three aspects: the capital cost, the material cost, and the overhead cost, where the capital costs for the two structures were estimated according to the production of D and silicon PVs with comparable capacity. According to their calculation, the estimated manufacturing cost of model A and model B was ≈\$30/m^2 and \$41/m^2, respectively.[127] Unlike the assumptions proposed by Cai et al., Chang et al. only considered structures and associated process sequences successfully demonstrated to produce functional laboratory-scale modules.[128] A process sequence that combines two demonstrated perovskite module sequences is estimated to be \$107/m^2, comparable with commercial CdTe technologies.[11] The result might underestimate the economic potential due to the choice of impractical production sequences, the use of costly materials, and slow-throughput deposition techniques (e.g., thermal evaporation). Different from the above two cases employing n-i-p structures, Song et al. selected a more manufacturable p-i-n module configuration with low-cost inorganic transporting materials that allow the process flow of an actual thin-film PV plant to be followed.[129] Based on the bottom–up cost model, they calculated the direct manufacturing cost of \$31.7/m^2, where material cost accounts for 76% of the total (**Figure** 7a,b). Actually, in the material constitute, 93.5% of material costs belong to the so-called balance of module components, including glass substrates, interconnection busbars, sealant, lamination film, edge-sealing frame, junction boxes, and wiring (Figure 7c).

Although achieving tremendous progress toward commercialization, PSMs have yet to harmonize the manufacturing process. Thus, a variety of device structures, alternative materials, and deposition methods could be considered for module fabrication. A sensitivity analysis explains how these various values affect the outcome under certain conditions. Song et al. analyzed the impact on the MSP when choosing different materials and corresponding fabrication processes. As shown in Figure S6 (Supporting Information), the replacement of electrode Al (used in reference) by Au, Ag, and graphite paste contributes to changes of MSP of +100.1, +2.3, and −0.6 ¢ W^{-1}, respectively. The use of scarce organic charge transport materials, poly(3-hexythiophene-2,5-diyl) (P3HT), PCBM, and spiro-OMeTAD instead of low-cost inorganic counterparts NiO and ZnO leads to cost increases of 1.2, 28.4, and 18.0 ¢ W^{-1}, respectively. Utilizing different deposition methods for perovskite films also varies the cost but with a small increase. For instance, the employment of a two-step solution, thermal vapor deposition, and two-step hybrid methods for perovskite layer fabrication merely leads to less than +0.5 ¢ W^{-1} compared to the single-step solution.[129]

The LCOE is defined as the ratio of the total lifecycle cost of a PV system to the total energy generated during its lifetime. The total cost is the sum of the annual cost of the

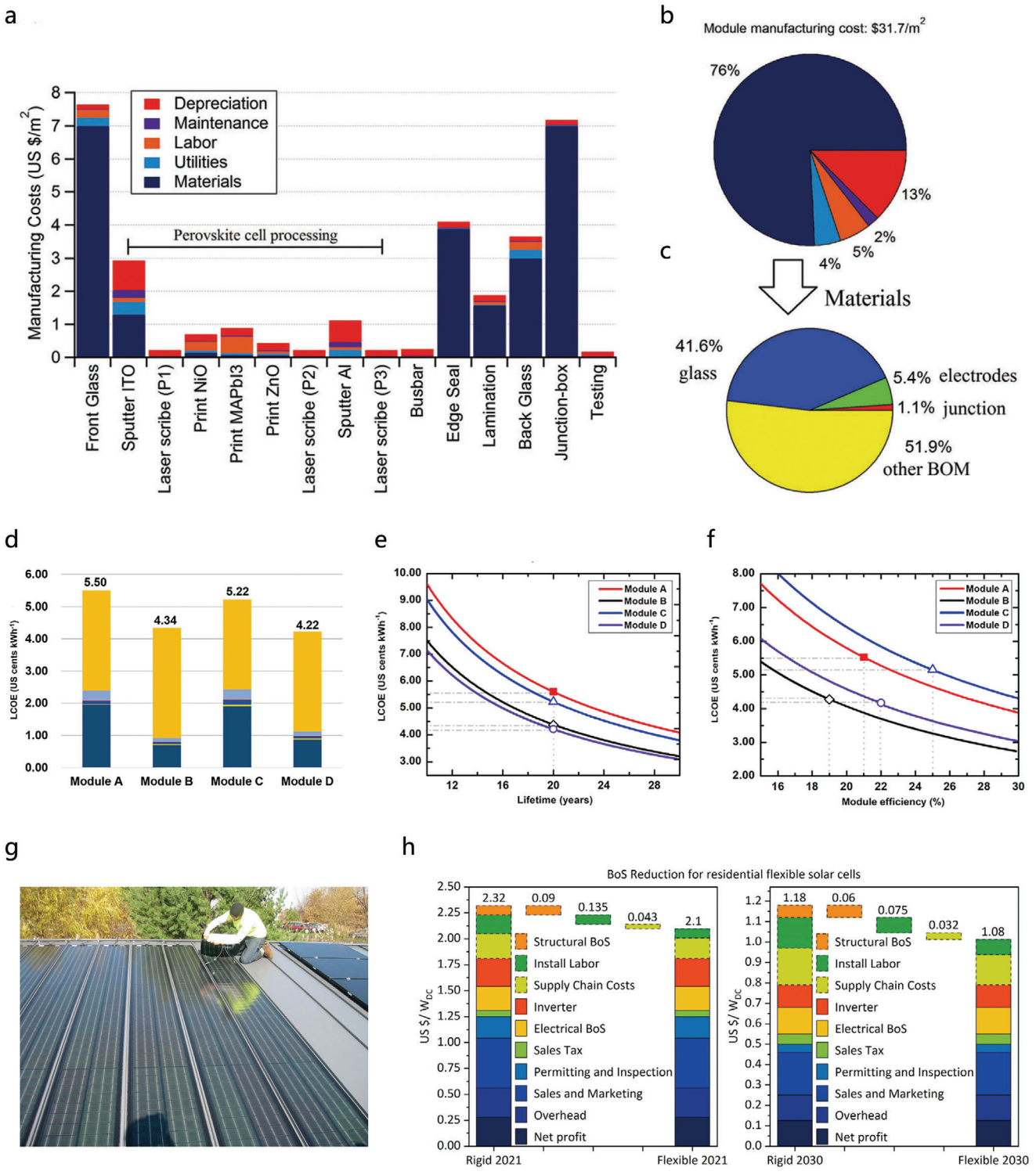

Figure 7. Cost analysis of typical perovskite modules. a) Step-by-step direct manufacturing costs of the reference monolithic PSMs. b) Direct manufacturing cost distribution. c) Materials cost breakdown of the reference module with a total manufacturing cost of $31.7/m^2. a–c) Reproduced with permission.[129] Copyright 2017, Royal Society of Chemistry. d) The comparison of LCOE. e) LCOE variation as functions of the module lifetime. f) LCOE variation as a function of the module efficiency. In Figure d–f, module A is composed of traditional silicon cells, module B is composed of planar perovskite cells, module C is composed of silicon/perovskite tandem cells and module D is composed of perovskite/perovskite tandem cells. d–f) Reproduced with permission.[130] Copyright 2018, Elsevier Inc. g) Flexible PV modules directly adhered to metal roofs, reproduced with permission.[132] Copyright 2015, IEEE. h) A detailed breakdown of the assumed cost reduction for the flexible scenario for the 2021 and 2030 scenarios for a 19.9% and 24% efficient module, respectively. Reproduced with permission.[57] Copyright 2023, Elsevier Inc.

system (C_t), which can be expressed by $C_t = I_t + O_t + F_t$, where I_t is the initial installation cost in year t ($I_t = 0$ when $t > 0$), including modules (typically based on the MSP model), inverters, other balance of system (BOS) equipment (e.g., racking, wiring, and tracking), and so on. O_t is the system operating cost, and F_t is the financing cost.[129] The LCOE of perovskite PVs was estimated to be 5.82 ¢ kWh^{-1} in Wichita, Kansas, with an assumed combination of a 16%-PCE and a 30-year system lifetime. Tandem structures demonstrate higher PCE without much-increased manufacturing cost. Li et al. performed a detailed cost analysis on two perovskite-based tandem modules (perovskite/c-Si and perovskite/perovskite tandems) compared with standard c-Si and single-junction PSMs. They found that perovskite PVs are competitive in the LCOE if the module lifetime is comparable with that of c-Si solar cells. The LCOE calculated for the two tandem modules were 5.22 and 4.22 ¢ kWh^{-1}, lower than the single-junction c-Si (5.50 ¢ kWh^{-1}) and perovskite devices (4.34 ¢ kWh^{-1}), revealing that tandem configurations have great potential for LCOE reduction in the future (Figure 7d).[130] Lifetime and PCEs are two primary factors that tightly reduce the LCOE value (Figure 7e,f). For example, with an increased lifetime from 10 to 20 years for a single-junction PSM, the LCOE decreases from 7.52 to 4.34 ¢ kWh^{-1} (Figure 7e).

When considering lightweight flexible PSMs to replace rigid counterparts, potential space for cost reduction still exists. Flexible PSMs are often claimed to have reduced manufacturing costs mainly originating from decreased substrate and labor costs. We compared the material cost of glass/ITO and PET/ITO at an enlarged scale that these substrate costs remain similar at this stage.[11,121,130] When considering the whole module manufacturing costs, flexible PSMs also exhibit a similar range to their rigid counterparts, and in some cases, the cost of flexible could be a little higher (e.g., 33.53 \$ m^{-2} for flexible device materials vs 31.7 \$ m^{-2} for rigid modules).[109,129]

Although the manufacturing cost reduction of flexible modules is not obvious, the BOS cost taken for LCOE could be competitively reduced. For the LCOE calculation, the initial installation cost I_t consists of modules, inverters, other BOS equipment, installation labor, project overhead costs, land fees, transportation, taxes, etc.[57,58,131–133] Light and flexible modules have reduced weight that allows for alternative mounting methods that, for instance, do not require additional racking used for heavy modules but can be placed conformally to the roof (Figure 7g).[131–133] This will contribute to a significant reduction in installation labor and racking costs. Metacarpa et al. reported up to a 47% cost reduction in hardware installation labor through the change from rigid to flexible PV modules.[133] In addition, rigid modules with glass substrates usually have a thickness exceeding 30 mm while flexible devices are significantly thinner, for example, flexible perovskite devices are less than 5 mm thick.[57] This brings in tighter packing density for flexible devices which permits a reduced transportation cost and storage cost, which is usually related to the land fees. According to the above analysis, Holzhey et al. summarized the upper bound of cost advantage for the BOS in Figure 7h. With the assumptions of the 2021 and 2030 scenarios, where LCOE is 11.9 and 5 ¢ KWh^{-1}, respectively, there is a significant cost advantage for the flexible substrate compared to the rigid counterparts.[57] To put it another way, for the 2021 scenario, a rigid perovskite module with 17% efficiency would need at least 24 years to become competitive with residential-installed silicon, while a light, flexible module with the same efficiency would only need to last 19 years due to the reduced cost.[57]

Detailed cost and LCOE summaries between different types of PV modules (such as CdTe, and CIGS) and PSMs with different configurations are shown in Tables S6,S7 (Supporting Information), providing an intuitive comparison for readers.

8.2. Toxicity Issues and Other Environmental Impacts

The use of toxic materials, especially lead, will require compliance with existing regulatory frameworks as has been discussed in the European Union's Restriction of Hazardous Substances (RoHS) Directive and Resource Conservation and Recovery Act (RCRA).[134–139] The RoHS Directive is the main regulation that prevents the distribution of potentially hazardous commercial electrical and electronic equipment (EEE) and has assisted in reducing 94% of the lead content of various electronics in Europe.[137] It sets the restriction for EEE where the maximum concentration of lead in homogeneous materials is 0.1% on a per-weight basis. According to the previous reports, PSCs with a typical thickness of 400 nm-perovskite (e.g., $MAPbI_3$ or $FAPbI_3$) would contain ≈0.4 g lead per square meter, corresponding roughly to the amount of 1-cm-thick natural soil of equivalent area that contains (**Figure 8a**).[135,137] When converted to mass fraction, the lead concentration was estimated to a value of 344 ± 4 mg k^{-1} g for PSCs fabricated on rigid glass substrates, lower than 0.1%, the safety limit imposed by the RoHS Directive (Figure 8b).[137] However, the RoHS Directive is not applicable in America, where the RCRA is established for hazardous waste management. RCRA aims to regulate the disposal of products and assesses hazardous waste based on leaching potential which is determined by the Toxicity Characteristic Leaching Procedure (TCLP). The leached lead concentrations are estimated by Moody et al. to be 14.2 ± 0.2 and 713 ± 5 mg L^{-1} on glass and PET substrates, respectively, both exceeding the 5 mg L^{-1} limit in regulations in RCRA (Figure 8c).[137] Thus, these substances require specific hazardous waste disposal rather than direct landfilling, which could add additional costs significantly. From the analysis above, lead-containing PSCs on rigid glass substrates have shown lower lead concentration below the limit in the RoHS Directive (even less than one-fiftieth of solders used in the silicon PV industry) and slightly higher concentration than the limit in RCRA, and can be even used as portable applications and merely requires additional waste-disposal costs that could be mitigated by recycling the modules.[131,137] From these aspects, some views are tempted to conclude that the amount of lead in perovskite modules is too low to create risk for human beings and the environment. However, different from the metallic form, the low amount of lead in perovskites is more toxic, even than its decomposition products like PbI_2. Bae et al. systematically investigated the toxicity potential of Pb-containing compounds that could be released accidentally from perovskite PV devices.[136] They conducted ecotoxicity bioassay and cytotoxicity bioassay battery toxicity tests to investigate the harmful effects of PSCs on the environment and human health based on four different species and human lung epithelia and hepatoma cells. They concluded the order of ecotoxicity

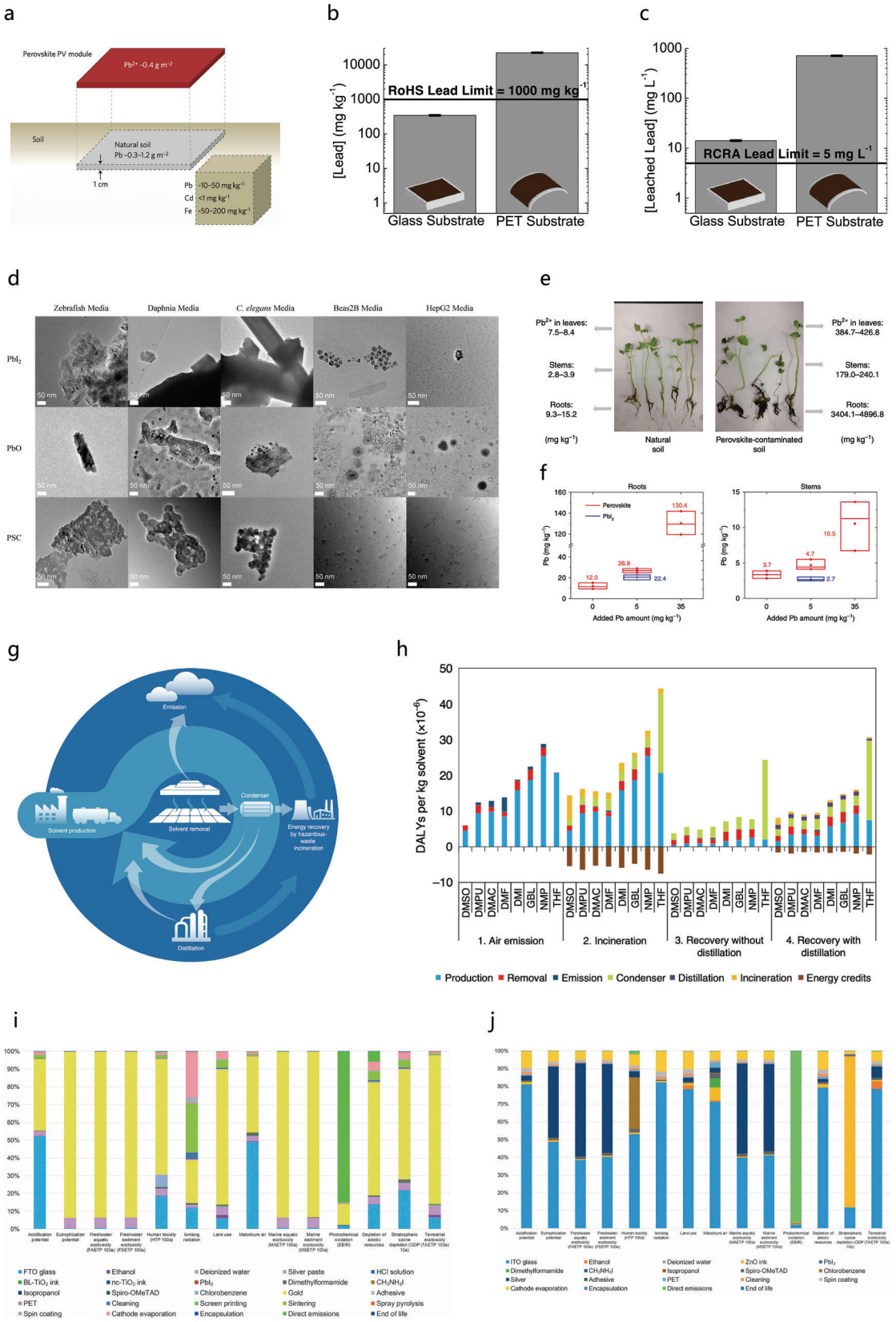

Figure 8. Toxicity of lead and used solvents. a) Amount of lead contained in a PSM and natural soil. Reproduced with permission.[135] Copyright 2016, Macmillan Publishers Limited. b). Total lead concentration of perovskite thin films on glass and PET substrates. c) TCLP leached lead concentration

and cytotoxicity was to be Pb^{2+} > $MAPbI_3$ > PbI_2 = lead oxide (PbO), where the PbI_2 and PbO represent the main lead-based degradation compounds of perovskites resulting from water and fire exposure.[136] Lead content could result in increased mortality and growth inhibition of species and pronounced deaths of human cells (Figure 8d), highlighting the non-negligible hazardous potentialities of the PSCs and their degradation products. In addition, the biological impact of lead from perovskites has also been investigated by J. Li et al.[138] They went into the ability of plants to uptake heavy metals from the ground, that is, the bioavailability of lead, in the existence of perovskite-containing medium and found that lead uptake by mint plants from the perovskite-contaminated soil was much higher than from natural soil or PbI_2-contaminated-only soil (Figure 8e,f), which was attributed to the pH change assisted by organic cations in perovskite. Therefore, lead from halide perovskite is more dangerous than other sources of lead, which is in agreement with the evidence obtained by Bea et al.[136] Thus, although the amount of lead-based perovskite is low, the harmful impact on animal and human health, as well as on plant growth and the entire ecosystem is non-negligible, which becomes an important obstacle for commercialization. To remove this roadblock, multiple strategies such as preventing the leakage or reducing the lead amount are proposed. One effective way to prevent leakage is to utilize lead adsorbers which could capture lead even when the devices are broken. For example, an encapsulation method based on an epoxy resin reduces the Pb leakage rate by a factor of 375 compared with the method based on a glass cover and a resin at the edges.[139] Additionally, recycling lead-based devices are considered an environmentally friendly way to not only reduce the lead risk but also reuse the components of frameworks when it comes to large-scale implementation, which will be discussed in the following section.

In addition to lead in perovskite PVs, the toxic solvents used in perovskite manufacturing also raise community concerns. Assumed by Vidal et al., the amount of solvent required for a blade-coated perovskite film is estimated to be 0.5 mL m^{-1}, indicating that 3500 liters of solvents are needed for 1 GW of solar power (an efficiency of 15% is assumed).[140] Organic solvents used in perovskite fabrication, like dimethylformamide (DMF), are always detrimental not only directly to human health but also to the environment, which irreversibly proposes harmful effects to the biologies. Vidal et al. analyzed the health and environmental impacts of eight solvents commonly used in perovskite processing, including DMF, DMSO, dimethylacetamide (DMAC), NMP, 1,3-dimethyl-2-imidazolidinone (DMI), gamma-butyrolactone (GBL), tetrahydrofuran (THF) and 1,3-dimethyl-3,4,5,6-tetrahydro-2(1H)-pyrimidinone (DMPU). The disability-adjusted life year (DALY), which is defined as a measure of disease burden composed of the sum of the years of life lost due to premature mortality in the population, and the years lost due to disability for people living with a health condition or its consequences, is used to evaluate the direct effects via human health toxicity and higher-order environmental effects impacting human health rather than human health toxicity directly.[140] For the case of direct emission to urban, DMF was found to have the highest DALYs, followed by DMAC, mainly due to fetotoxicity, while DMSO showed the least DALYs. Vidal et al. then implemented the full LCA to analyze the impact during the whole procedures of perovskite PV manufacturing including industrial solvent production, use, removal, and end-of-life (EOL) treatment (Figure 8g). For the EOL, four potential scenarios are shown: 1) direct air emission of the solvents, 2) incineration of condensed solvent with energy production, 3) recovery of the condensed solvents without further treatment, 4) distillation for solvent recovery and unrecovered fraction incinerated. The middle term like solvent removal might need energy input that could further lead to concerns about global warming and fine particulate matter. From Figure 8h, the incineration treatment for the EOL without energy recovery is always harmful to the environment, even higher than the direct emission of solvents into the atmosphere. DMSO in all scenarios exhibits the lowest human health and environmental impacts but it usually cannot be used as a single solvent. Since the total solvent quantity is marginal even at the industrial scale, Vital et al. concluded that there would not be likely a substantial impact on human health due to solvent use, consistent with the view by Wagner et al.[134] But further seeking greener processes could reduce the harmful impact of solvents, especially for DMF. In addition, the solvent recovery process is always more environmentally friendly than incineration even with energy recovery, which encourages the utilization of an efficient recovery process.

Except for the toxic lead-containing perovskite and solvents, Gong et al. developed comprehensive life cycle inventories (LCIs) for all components used in the modules.[141] Based on LCIs, they provided 16 common life cycle impact indicators, including acidification, eutrophication, freshwater aquatic ecotoxicity, freshwater sediment ecotoxicity, human toxicity, ionizing radiation, and so on.[141] The typical indicators of two types of PSMs (TiO_2 and ZnO-based) are shown in Figure 8i,j, where the gold cathode in TiO_2-based PSMs is the most significant contributor to eutrophication (93%), freshwater aquatic ecotoxicity (93%), freshwater sediment ecotoxicity (93%), human toxicity (65%), land use (76%), marine aquatic ecotoxicity (93%), and marine sediment

perovskite thin films on glass and PET substrates. b,c) Reproduced with permission.[137] Copyright 2020, Elsevier Inc. d) Characterization of PSC and its degradation products in ecotoxicity (Zebrafish, Daphnia, and C. elegans media) and cytotoxicity test media (i.e., Beas2B and HepG2 media). Transmission electron microscope images are shown with a scale bar of 50 nm. Reproduced under the terms of the CC BY Creative Commons Attribution 4.0 International License (http://creativecommons.org/licenses/by/4.0/).[136] Copyright 2019, The Authors, published by Springer Nature. e) The picture of mint plants grown on control soil and 250 mg k^{-1} g Pb^{2+} perovskite-contaminated soil. The ranges of lead content measured in the leaves, stems, and roots are reported on the side of each picture. f) Lead concentration in different parts of mint plants: roots, and stems. e,f) Reproduced under the terms of the CC BY Creative Commons Attribution 4.0 International License (http://creativecommons.org/licenses/by/4.0/).[138] Copyright 2020, The Authors, published by Springer Nature. g) LCA system boundary schematic showing possible pathways for the perovskite PV production. h) LCA of eight aprotic solvents for perovskite film manufacturing with four potential scenarios for EOL. Negative values indicate energy credits. g,h) This is a U.S. government work and not under copyright protection in the U.S. i) Environmental profile of 1 m^2 of the TiO_2 module. j) Environmental profile of 1 m^2 of the ZnO module. i,j) Reproduced with permission.[141] Copyright 2015, Royal Society of Chemistry.

ecotoxicity (93%), while the replacement by silver could significantly alleviate this issue.[141]

Additionally, two sustainable indicators are also very important in the LCA: the energy payback time (EPBT) and the greenhouse gas (GHG) emission factor, which are perspectives to quantitatively estimate energy consumption and environmental emissions.[141–144] The EPBT of a PSM is defined as the ratio between the total primary energy consumption and the annual electricity generation, where the total primary energy consumption includes the energy embedded in raw materials, the energy consumed in manufacturing, and the energy consumed in end-of-life processing.[141–143] The GHG emission factor indicates the GHG emissions per kWh of electric power generated by the PSMs across the whole lifetime and it can be obtained if the carbon footprint is divided by the electricity generated. The carbon footprint is also contributed by raw materials, energy consumption, and direct emissions during manufacturing and landfilling. Based on the LCIs, these values can be easily calculated, where the PSMs usually possess a smaller EPBH and higher GHG factors compared to mature c-Si PV technology due to their different manufacturing routes.

8.3. Resource Demands and Recycling Potential

As the perovskite PV industry is scaling up, the resource abundance is now supposed to be investigated quantitatively for a thorough evaluation of the material demand and potential supply risks. Wagner et al. investigated the resource demand for a TW-scale perovskite PV production by considering two factors that reflect supply criticality, namely mining capacity for minerals, as well as production capacity for synthetic materials.[134] The mining capacity is used to measure the availability of each inorganic material for large-scale perovskite PV manufacturing. For a further clear illustration of mining capacity, another two factors are defined: demand-production-ratio (DPR) which relates the material demand for the production of 1 TW a^{-1} PV modules to current annual primary production, bound-reserves-ratio (BRR) which relates the material assets that are bound in global PV installations to the known reserves of the respective material. Inorganic materials like cesium (Cs) and indium (In) are associated with high supply criticality and these two factors provide an intuitive reflection. The DPR factor, focusing on inorganic material scarcity is shown in **Figure 9a**, that Au (DPR) and In (DPR) used in electrodes and Cs (DPR) used in perovskite have the highest values of 195%, 457%, and 1122%. BRR (a 25-year lifetime is assumed) shows a similar trend to DPR, but when the reserve is relatively sufficient, this value could become lower. For example, the Cs reserves are relatively larger although with a low mining capacity, the BRR factor is reduced to a moderate level compared to its high DPR level (Figure 9b).[134]

While for the organic components of perovskite (e.g., charge transport materials, MA, FA, and so on), which mainly consist of carbon, nitrogen, and hydrogen atoms, just considering the elemental availability is not sufficient. The complexity of the synthesis and current technological readiness of industrial production needs to be assessed, which can be measured by the technological readiness level (TRL). TRL reflects the technological maturity and feasibility of industrial production, and no TRL means that, currently, there is no technological concept for industrial production. The commonly used organic materials are included in Figure 9c, with the *x*-axis representing TRL and the *y*-axis representing the necessary scaling for 1 TW a^{-1} perovskite magnitude. Among these organic components, only PEDOT: PSS is mature and already well-established for industrial production while spiro-OMeTAD and PTAA do not possess matched scaling routes. Besides, for a 1 TW a^{-1} scale perovskite scale, the solvent consumption seems to be enough that all the necessary solvent scaling demand falls within a production increase below 20% (Figure 9d).[134]

The recycling of potential components of PSMs not only reduces the use of scarce resources but also creates economic benefits from recycled materials (**Figure 10a**). Currently, not all the parts in a module are easy to recycle or some recycling strategies is not cost-effective, thus a stricter materials and device design for the circular economy is important and should occur before commercialization. Now, TCO substrates and encapsulation components make up the primary cost of the module material when noble metal electrodes are not used. Song et al. estimated the glass used in the module made up 41.6% of the total material cost and Chen et al. got a similar conclusion with different components.[129,145] Besides, lead-based salts like PbI_2 also have a relatively large cost percentage while what's more concerning is its toxicity. Thus, the TCO-based substrates, back encapsulation glass, and lead-containing parts attract the most recycling attention. By applying acidic cation exchange resin, Chen et al. separated the PbI_2 from decommissioned modules with a recycling efficiency of 99.2%, by transforming lead to a soluble lead nitrate ($Pb(NO_3)_2$) salts and then precipitating it to desired PbI_2 (Figure 10b).[145] For the recycling of glass substrates and covers, thermal delamination was adopted to disassemble the encapsulated modules. Devices based on recycled lead iodide and recycled transparent conductors showed a comparable performance (Figure 10c). The material consumption for recycling the PSM was \$4.24/m^2 if these materials were used only once and the cost could further be decreased to \$1.35/m^2 if reusing DMF and resin five times, and it saved the total value of recycled components, including front ITO/glass, PbI_2, and back cover glass, to ≈\$12/m^2. The recycling of other parts like the TCLs and back metal electrodes is strongly dependent on the device configuration. For example, the reuse of noble metals like gold is valuable while sometimes becoming useless for inexpensive counterparts like Al and Cu. The reuse of organic CTLs is usually different to perform because these commercial films (like spiro-OMeTAD) may contain many elements whose recyclability has been rarely studied (Figure 10d).[146] Wang et al. demonstrated a so-called "one-key-reset" recycling method to simultaneously collect all the functional layers from a PSC. This method utilized a bleaching solution to spontaneously separate the perovskite layer from the spiro-OMeTAD layer due to solvent polarity and allow detachment of the gold electrode and SnO_2-coated ITO/glass substrates.[146] This approach paces the way to dramatically lower the levelized cost of energy of perovskite PVs and enhance their competitiveness in future energy markets.

In addition to creating dramatic economic benefits, the recycling utilization of components of PSMs also protects the environment, such as decreasing energy consumption and greenhouse gas emissions. Reusing TCO substrates and related CTLs

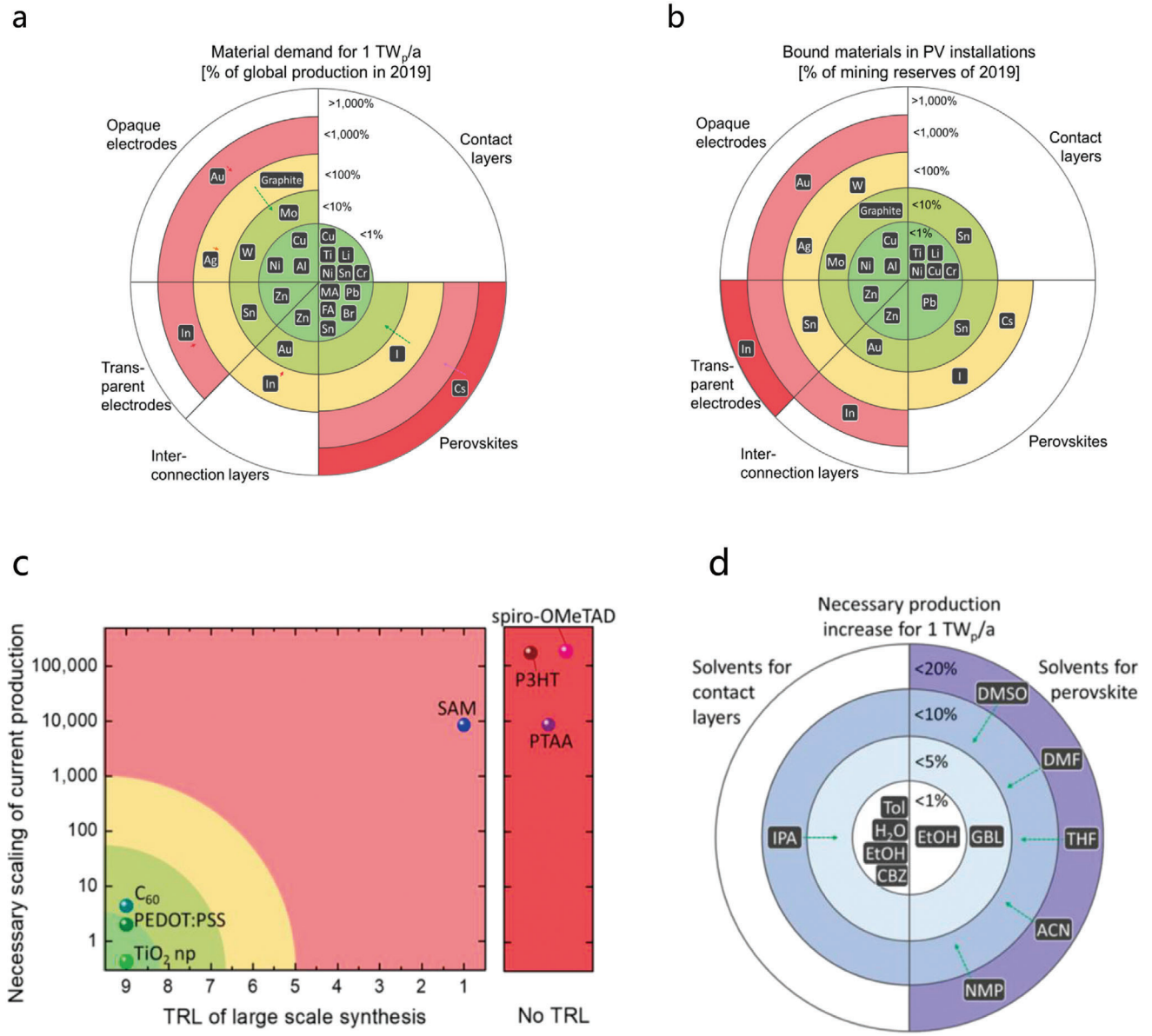

Figure 9. Material demand and required increase for TW-scale perovskite PV industry. a) Supply risk assessment of inorganic materials used for TW-scale perovskite PV. The organic materials MA and FA are been also added for comparability. Dashed arrows illustrate the potential to reduce the DPR by scaling the production. b) BRR of different elements used in PSMs. c) Necessary scaling of production and increase in TRL of the industrial synthesis of synthetic materials for a 1 TW a^{-1} perovskite PV production. d) Necessary increment of solvent production for the production of 1 TW a^{-1} perovskite PV. Dashed arrows illustrate the potential to reduce consumption by solvent recycling. a–d) Reproduced under the terms of the CC BY Creative Commons Attribution 4.0 International License (http://creativecommons.org/licenses/by/4.0/).[134] Copyright 2023, The Authors, posted as arXiv:2306.13375.

is one straightforward method to reduce EPBT and GHG emission factors, which effectively reduces energy consumption and environmental effects. Tian et al. compared six kinds of PSCs with different substrates, CTLs, configurations, and electrodes, and analyzed both the landfill and recycling EOL scenarios.[142] For example, for the LBSO module which employed lanthanum (La)-doped barium stannate ($BaSnO_3$) as ETL, up to 72.3% of primary energy is saved by reusing LBSO-coated FTO substrates and Cu electrodes. For Other types of PSCs like metal oxide-based modules, only 15.5% of the primary energy is saved. The differences mainly originate from the different energy consumption during assembly. The EPBT and GHG emission factors are linearly dependent on the mentioned primary energy consumption, which is cut down by a similar percentage for six types of PSCs. The EPFT and GHG emission factors are thoroughly compared with existing PV technologies, including c-Si modules, poly-crystalline silicon (p-Si) modules, ribbon silicon (ribbon-Si) modules, CdTe modules, OPV modules and two alternative PSMs (the TiO_2 module and the ZnO module) in Tian et al.'s discussion, where the best-recycled module architecture (SnO_2 type) exhibit an extremely small energy payback time of 0.09 years and a GHG emission factor of 13.4 g CO_2 equivalent

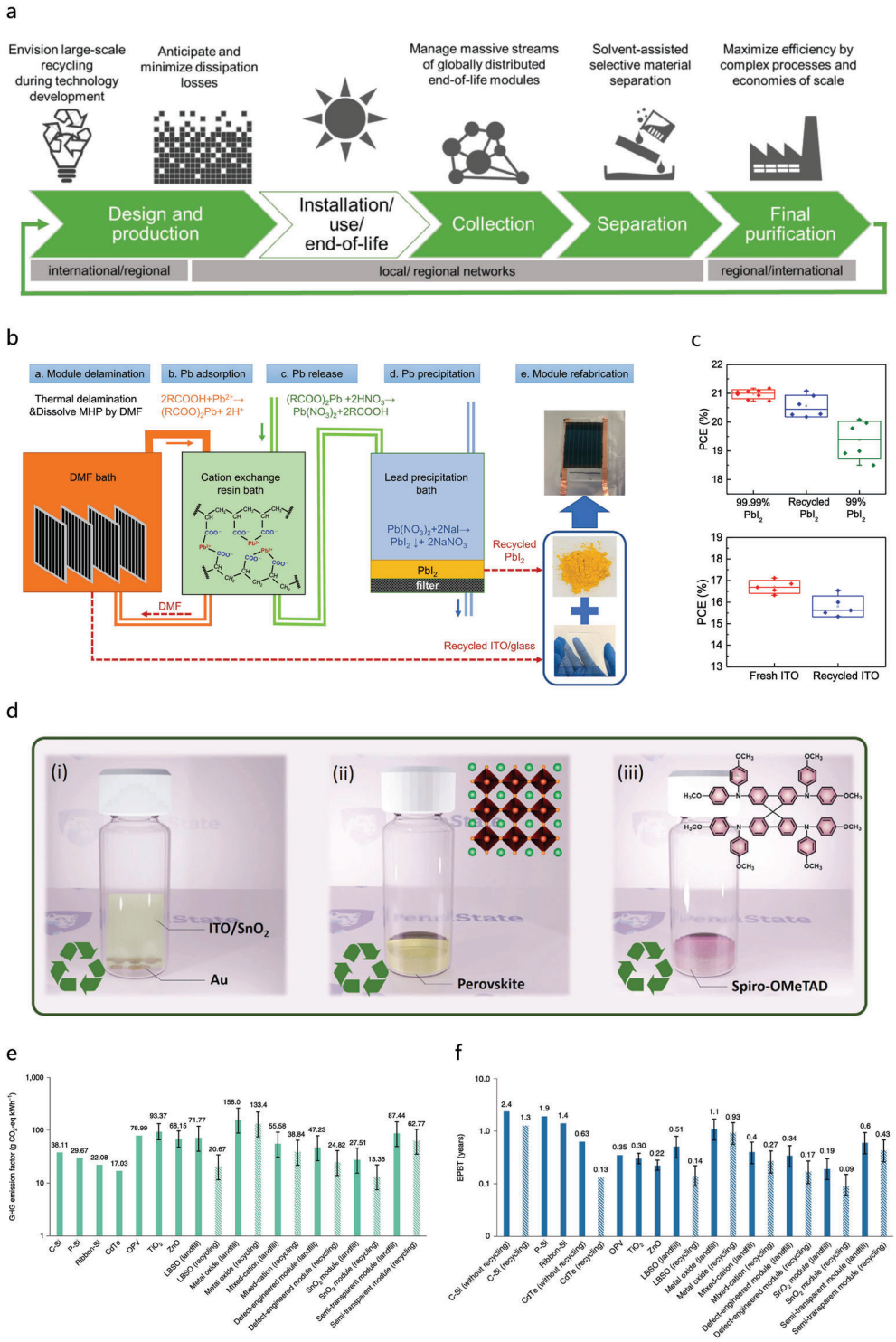

Figure 10. Recycling potential of PSMs. a) Guidelines for perovskite PV recycling. Reproduced under the terms of the CC BY Creative Commons Attribution 4.0 International License (http://creativecommons.org/licenses/by/4.0/).[134] Copyright 2023, The Authors, posted as arXiv:2306.13375. b) Roadmap for recycling of PSMs for substrates and lead. c) PCE of PSCs fabricated with commercial 99.99% PbI_2, recycled PbI_2, and commercial 99% PbI_2 and PCE of PSMs fabricated on fresh ITO and recycled ITO. b,c) Reproduced under the terms of the CC BY Creative Commons Attribution 4.0 International License (http://creativecommons.org/licenses/by/4.0/).[145] Copyright 2021, The Authors, Published by Springer Nature. d) three components of (i) Au and SnO_2-coated ITO/glass (ITO/SnO_2), (ii) liquefied perovskite, and (iii) nonpolar solvent-dissolved spiro-OMeTAD have been obtained, reproduced with permission.[146] Copyright 2021, Elsevier Inc. e) Comparison of GHG emission factors among 13 PV modules based on different technologies. f) Comparison of EPBT among 13 PV modules based on different technologies. e,f) Reproduced with permission from. Ref. [142]. Copyright 2021, Springer Nature Limited.

per kWh (Figure 10e,f).[141,142] Thus, the effective recycling of PSMs demonstrates great potential for module cost and LCOE reduction.

9. Perspective

In this manuscript, we start with the challenges perovskite modules are facing toward commercialization and propose the corresponding strategies. In general, to achieve practical applications, the LCOE of PSMs should be reduced to a comparable level with state-of-the-art PV technologies, which proposes strict demands for the PCE, lifetime, and cost. In addition to the main concerns, we also put forward several other subordinate challenges or developing aspects that could facilitate commercialization. The first aspect is the toxicity issue at the product level as well as during fabrication processes. The second is the attainment of highly efficient perovskite-based tandem modules, which could further accelerate the LCOE reduction.

Almost all high-performance PSMs utilize lead-containing components because of their unique and irreplaceable optoelectronic properties. Due to the water-soluble nature, the leakage problem of toxic lead needs to raised concerns although the amount of lead contained is relatively limited. One practical approach mentioned above is to use built-in materials like polymers for delicate encapsulation. A new device structure that incorporates a low-cost mesoporous sulfonic acid-based resin into perovskites as a scaffold immobilizes lead ions inside even if perovskites are exposed to rainwater.[147] These results strongly suggest that perovskite PV products can be deployed with minimal lead leakage with appropriate encapsulation employed. In addition, the recycling of lead and other valuable components of the scrapped modules will not only help to reduce the negative impact on the environment but also save the use of scarce resources.[142,146] More investigation should be devoted to finding a cost-effective and feasible approach to effectively recycle the worthwhile parts. Apart from the lead leakage, the toxicity of commonly used solvents during fabrication, such as DMF, and NMP, which are injurious to health because of toxicity, ability to penetrate the skin, and carcinogenicity, is also one prominent problem.[142] The EOL treatment of solvents needs careful consideration that incineration sometimes creates more pronounced negative impacts on the environment than direct emission although they can produce excess energy.[139] Several groups are seeking green solvent systems for toxicity reduction: one approach is to replace hazardous reagents with those exhibiting reduced toxicity like ethanol, and the second is to use a solvent with very low vapor pressures, like ionic liquids, which limits the emission to the atmosphere.[139,148,149]

Further improvement of PCE plays a vital role in LCOE reduction. Thus, high-efficiency tandem solar cells can be an effective approach in the future, as they do not induce much additional area-related BOS cost. This feature could make the PCE gain in tandem prevail over the other additional fabrication costs. The bandgap-tunable nature makes perovskites a promising candidate to compensate with various bottom cells like c-Si, CIGS, and low-bandgap perovskites. Due to the high PCE and mature industry of silicon, employing c-Si solar cells to fabricate perovskite-silicon tandem modules has an undisputed prospect. According to the calculation by Zafoschnig et al., the LCOE of the perovskite-silicon tandem module is estimated to be lower than that of a commercial c-Si module and a single-junction PSM if the PCE exceeds 24% and lifetime performs at the comparable level with silicon (Figure S7, Supporting Information).[150] The record PCE of perovskite-silicon tandems has reached 33.9%, surpassing other types of tandems based on perovskites.[3,13] However, some issues remain and are supposed to be further unified or solved. The adoption of wide-bandgap perovskites (as top cells) exacerbates the stability of real-world energy yields, challenging the progression of widespread commercialization. The phase instability, for example, the migration of bromide and iodide ions in wide-bandgap perovskites becomes deteriorated, leading to the segregation of bromide-rich and iodide-rich perovskite phases. The strain-related instability also requires attention as the mismatch between the perovskite-silicon interface exceeds that of glass as the CTE of silicon is down to 0.26×10^{-5} K^{-1}.[151] In addition, choosing what types of c-Si as the bottom cells has not been unified. Tunnel oxide passivated contact (TOPCon)-type and heterojunction (HJT)-type c-Si solar cells can both realize high PCEs and are often chosen as the bottoms. The "n-i-p" structure (in the view of perovskites) of TOPCon may render perovskite-TOPCon tandems to develop out of the mainstream because currently the top wide-bandgap perovskite solar cells mainly utilize inverted structures. Finally, highly efficient c-Si cells have texturization (typically 0.5–10 μm) on both sides for improved light trapping.[151–153] Depositing perovskite on this rough surface will be a challenging task. Vapor-based deposition like thermal evaporation serves as one of the alternatives but faces the issue of increased expense, complexity, and decreased output. New attempts still need to be proposed for building a bridge between the laboratory and industry.

Supporting Information

Supporting Information is available from the Wiley Online Library or from the author.

Acknowledgements

This work was jointly supported by the National Natural Science Foundation of China (No. 51925204), Carbon Peaking and Carbon Neutrality Science and Technology Innovation Fund of Jiangsu Province (BK20220035), Major Research Plan of the National Natural Science Foundation of China (No. 92262305), National Key Research and Development Program of China (No.2022YFA1404704). J.Z. acknowledges support from the XPLORER PRIZE. S.C. appreciates the support from the National Natural Science Foundation of China (No. 52372196). P.Z. acknowledges the 2021 Jiangsu Mass Entrepreneurship and Innovation Talent Program (grant No. JSSCBS 20210051) and Y.Z. for the helpful discussion.

Conflict of Interest

The authors declare no conflict of interest.

Keywords

commercialization, modules, perovskites, solar cells

Received: July 24, 2023
Revised: December 23, 2023
Published online:

[1] A. Kojima, K. Teshima, Y. Shirai, T. Miyasaka, *J. Am. Chem. Soc.* **2009**, *131*, 6050.
[2] M. A. Green, A. Ho-Baillie, H. J. Snaith, *Nat. Photonics* **2014**, *8*, 506.
[3] NREL, Best Research-Cell Efficiencies, https://www.nrel.gov/pv/assets/pdfs/best-research-cell-efficiencies.pdf, accessed, December **2023**.
[4] Z. Li, T. R. Klein, D. H. Kim, M. Yang, J. J. Berry, M. F. A. M. Van Hest, K. Zhu, *Nat. Rev. Mater.* **2018**, *3*, 18017.
[5] N.-G. Park, K. Zhu, *Nat. Rev. Mater.* **2020**, *5*, 333.
[6] NREL, Champion Module Efficiencies, https://www.nrel.gov/pv/assets/pdfs/champion-module-efficiencies.pdf, accessed, December **2023**.
[7] M. A. Green, K. Emery, *Prog. Photovoltaics* **1993**, *1*, 25.
[8] S.-W. Lee, S. Bae, D. Kim, H.-S. Lee, *Adv. Mater.* **2020**, *32*, 2002202.
[9] L. Meng, J. You, Y. Yang, *Nat. Commun.* **2018**, *9*, 5265.
[10] P. Culík, K. Brooks, C. Momblona, M. Adams, S. Kinge, F. Maréchal, P. J. Dyson, M. K. Nazeeruddin, *ACS Energy Lett.* **2022**, *7*, 3039.
[11] B. Smith, M. Woodhouse, K. Horowitz, T. Silverman, J. Zuboy, R. Margolis, NREL/TP-7A40-78173, 2021, 1829459, MainId: 32082.
[12] G. Grancini, C. Roldán-Carmona, I. Zimmermann, E. Mosconi, X. Lee, D. Martineau, S. Narbey, F. Oswald, F. De Angelis, M. Graetzel, M. K. Nazeeruddin, *Nat. Commun.* **2017**, *8*, 15684.
[13] M. Green, E. Dunlop, M. Yoshita, N. Kopidakis, K. Bothe, G. Siefer, X. Hao, *Prog. Photovoltaics, Res. Appl.* **2024**, *32*, 3.
[14] *Overview of Utmolight company*, http://www.utmolight.com, accessed: December **2023**.
[15] F. Matteocci, S. Razza, F. Di Giacomo, S. Casaluci, G. Mincuzzi, T. M. Brown, A. D'epifanio, S. Licoccia, A. Di Carlo, *Phys. Chem. Chem. Phys.* **2014**, *16*, 3918.
[16] W. Luo, C. E. Clement, Y. S. Khoo, Y. Wang, A. M. Khaing, T. Reindl, A. Kumar, M. Pravettoni, *Renewable Energy* **2021**, *177*, 327.
[17] A. Mei, Y. Sheng, Y. Ming, Y. Hu, Y. Rong, W. Zhang, S. Luo, G. Na, C. Tian, X. Hou, Y. Xiong, Z. Zhang, S. Liu, S. Uchida, T.-W. Kim, Y. Yuan, L. Zhang, Y. Zhou, H. Han, *Joule* **2020**, *4*, 2646.
[18] M. V. Khenkin, E. A. Katz, A. Abate, G. Bardizza, J. J. Berry, C. Brabec, F. Brunetti, V. Bulović, Q. Burlingame, A. Di Carlo, R. Cheacharoen, Y.-B. Cheng, A. Colsmann, S. Cros, K. Domanski, M. Dusza, C. J. Fell, S. R. Forrest, Y. Galagan, D. Di Girolamo, M. Grätzel, A. Hagfeldt, E. von Hauff, H. Hoppe, J. Kettle, H. Köbler, M. S. Leite, S. (Frank) Liu, Y.-L. Loo, V. Turkovic, *Nat. Energy* **2020**, *5*, 35.
[19] R. Azmi, E. Ugur, A. Seitkhan, F. Aljamaan, A. S. Subbiah, J. Liu, G. T. Harrison, M. I. Nugraha, M. K. Eswaran, M. Babics, Y. Chen, F. Xu, T. G. Allen, A. U. Rehman, C.-L. Wang, T. D. Anthopoulos, U. Schwingenschlögl, M. De Bastiani, E. Aydin, S. De Wolf, *Science* **2022**, *376*, 73.
[20] *Overview of Microquanta company*, http://www.microquanta.com, accessed: December **2023**.
[21] G. Nazir, S.-Y. Lee, J.-H. Lee, A. Rehman, J.-K. Lee, S. I. l. Seok, S.-J. Park, *Adv. Mater.* **2022**, *34*, 2204380.
[22] *Overview of GCL company*, http://www.gcl-perovskite.com/wm/, accessed: December **2023**.
[23] *Overview of Wondersolar company*, http://wondersolar.cn/en/nd.jsp?id=11, accessed: November **2023**.
[24] E. Andy, *Nature* **2019**, *570*,429.
[25] Toshiba's polymer film-based perovskite module, https://www.pv-magazine.com/2023/08/25/toshiba-claims-16-6-efficiency-for-polymer-film-based-large-area-perovskite-solar-module, accessed: November **2023**.
[26] Toshiba's polymer film-based perovskite module, https://news.toshiba.com/press-releases/press-release-details/2021/Toshibas-Polymer-Film-Based-Perovskite-Large-Area-Photovoltaic-Module-Reaches-Record-Power-Conversion-Efficiency-of-15.1/default.aspx, accessed: November **2023**.
[27] Toshiba's glass-based perovskite module, https://www.global.toshiba/ww/news/corporate/2018/08/tp0901.html, accessed: November **2023**.
[28] Panasonic's glass-based perovskite module, https://holdings.panasonic/jp/corporate/technology/technology-journal/pdf/v6801/p0109.pdf, accessed, November **2023**.
[29] *Overview of Solaronix company*, https://www.solaronix.com, accessed: November **2023**.
[30] https://www.engineering.com/story/first-solar-achieves-industrys-best-pv-degradation-rate, accessed: November **2023**.
[31] *Overview of Solaronix company*, https://www.diva-portal.org/smash/get/diva2:1305998/FULLTEXT01.pdf, accessed: November **2023**.
[32] J. Bing, L. G. Caro, H. P. Talathi, N. L. Chang, D. R. Mckenzie, A. W. Y. Ho-Baillie, *Joule* **2022**, *6*, 1446.
[33] F. Lang, N. H. Nickel, J. Bundesmann, S. Seidel, A. Denker, S. Albrecht, V. V. Brus, J. Rappich, B. Rech, G. Landi, H. C. Neitzert, *Adv. Mater.* **2016**, *28*, 8726.
[34] G. Eder, G. Peharz, R. Trattnig, P. Bonomo, E. Saretta, F. Frontini, C. S. P. Lopez, H. R. Wilson, J. Eisenlohr, N. M. Chivelet, S. Karlsson, N. Jakica, A. Zanelli, Coloured BIPV: Market, Research and Development. **2019**.
[35] S. Pescetelli, A. Agresti, G. Viskadouros, S. Razza, K. Rogdakis, I. Kalogerakis, E. Spiliarotis, E. Leonardi, P. Mariani, L. Sorbello, M. Pierro, C. Cornaro, S. Bellani, L. Najafi, B. Martín-García, A. E. Del Rio Castillo, R. Oropesa-Nuñez, M. Prato, S. Maranghi, M. L. Parisi, A. Sinicropi, R. Basosi, F. Bonaccorso, E. Kymakis, A. Di Carlo, *Nat. Energy* **2022**, *7*, 597.
[36] Throughput of CdTe PV modules, High-throughput manufacturing of thin-film CdTe photovoltaic modules https://www.nrel.gov/docs/legosti/fy97/21598.pdf, accessed: November **2023**.
[37] M. Saliba, M. Stolterfoht, C. M. Wolff, D. Neher, A. Abate, *Joule* **2018**, *2*, 1019.
[38] Y. Deng, S. Xu, S. Chen, X. Xiao, J. Zhao, J. Huang, *Nat. Energy* **2021**, *6*, 633.
[39] A. Mei, X. Li, L. Liu, Z. Ku, T. Liu, Y. Rong, M. Xu, M. Hu, J. Chen, Y. Yang, M. Grätzel, H. Han, *Science* **2014**, *345*, 295.
[40] Y. Deng, X. Zheng, Y. Bai, Q. Wang, J. Zhao, J. Huang, *Nat. Energy* **2018**, *3*, 560.
[41] R. Patidar, D. Burkitt, K. Hooper, D. Richards, T. Watson, *Mater. Today Commun.* **2020**, *22*, 100808.
[42] J. H. Heo, M. H. Lee, M. H. Jang, S. H. Im, *J. Mater. Chem. A* **2016**, *4*, 17636.
[43] X. Peng, J. Yuan, S. Shen, M. Gao, A. S. R. Chesman, H. Yin, J. Cheng, Q. Zhang, D. Angmo, *Adv. Funct. Mater.* **2017**, *27*, 1703704.
[44] C. Chen, J. Chen, H. Han, L. Chao, J. Hu, T. Niu, H. Dong, S. Yang, Y. Xia, Y. Chen, W. Huang, *Nature* **2022**, *612*, 266.
[45] Q. Chen, H. Zhou, Z. Hong, S. Luo, H.-S. Duan, H.-H. Wang, Y. Liu, G. Li, Y. Yang, *J. Am. Chem. Soc.* **2014**, *136*, 622.
[46] M. Liu, M. B. Johnston, H. J. Snaith, *Nature* **2013**, *501*, 395.
[47] R. A. Z. Razera, D. A. Jacobs, F. Fu, P. Fiala, M. Dussouillez, F. Sahli, T. C. J. Yang, L. Ding, A. Walter, A. F. Feil, H. I. Boudinov, S. Nicolay, C. Ballif, Q. Jeangros, *J. Mater. Chem. A* **2020**,*8*, 242.
[48] A. Farag, T. Feeney, I. M. Hossain, F. Schackmar, P. Fassl, K. Küster, R. Bäuerle, M. A. Ruiz-Preciado, M. Hentschel, D. B. Ritzer, A. Diercks, Y. Li, B. A. Nejand, F. Laufer, R. Singh, U. Starke, U. W. Paetzold, *Adv. Energy Mater.* **2023**, *13*, 2203982.
[49] D. Beynon, E. Parvazian, K. Hooper, J. Mcgettrick, R. Patidar, T. Dunlop, Z. Wei, P. Davies, R. Garcia-Rodriguez, M. Carnie, M. Davies, T. Watson, *Adv. Mater.* **2023**, *35*, 2208561.
[50] X. Dai, S. Chen, Y. Deng, A. Wood, G. Yang, C. Fei, J. Huang, *PRX Energy* **2022**, *1*, 013004.
[51] M. Zhang, Z. Lin, *Energy Environ. Sci.* **2022**, *15*, 3152.

[52] S. Sánchez, L. Pfeifer, N. Vlachopoulos, A. Hagfeldt, *Chem. Soc. Rev.* **2021**, *50*, 7108.
[53] C. O. Teixeira, D. Castro, L. Andrade, A. Mendes, *Energy Sci. Eng.* **2022**, *10*, 1478.
[54] J. J. Berry, J. Van De Lagemaat, M. M. Al-Jassim, S. Kurtz, Y. Yan, K. Zhu, *ACS Energy Lett.* **2017**, *2*, 2540.
[55] L. Qiu, L. K. Ono, Y. Qi, *Mater. Today Energy* **2018**, *7*, 169.
[56] P. Jiang, T. W. Jones, N. W. Duffy, K. F. Anderson, R. Bennett, M. Grigore, P. Marvig, Y. Xiong, T. Liu, Y. Sheng, L. Hong, X. Hou, M. Duan, Y. Hu, Y. Rong, G. J. Wilson, H. Han, *Carbon* **2018**, *129*, 830.
[57] P. Holzhey, M. Prettl, S. Collavini, N. L. Chang, M. Saliba, *Joule* **2023**, *7*, 257.
[58] J. Liu, T. Ye, D. Yu, S. F. Liu, D. Yang, *Angew. Chem., Int. Ed.* **2023**, *62*, 202307225.
[59] N. T. K. Thanh, N. Maclean, S. Mahiddine, *Chem. Rev.* **2014**, *114*, 7610.
[60] H. Hu, Z. Ren, P. W. K. Fong, M. Qin, D. Liu, D. Lei, X. Lu, G. Li, *Adv. Funct. Mater.* **2019**, *29*, 1900092.
[61] S. Chen, X. Xiao, H. Gu, J. Huang, *J. Sci. Adv.* **2021**, *7*, eabe8130.
[62] J.-E. Kim, Y.-S. Jung, Y.-J. Heo, K. Hwang, T. Qin, D.-Y. Kim, D. Vak, *Sol. Energy Mater. Sol. Cells* **2018**, *179*, 80.
[63] X. Li, D. Bi, C. Yi, J.-D. Décoppet, J. Luo, S. M. Zakeeruddin, A. Hagfeldt, M. Grätzel, *Science* **2016**, *353*, 58.
[64] S. Tang, Y. Deng, X. Zheng, Y. Bai, Y. Fang, Q. Dong, H. Wei, J. Huang, *Adv. Energy Mater.* **2017**, *7*, 1700302.
[65] Y. Y. Kim, T.-Y. Yang, R. Suhonen, A. Kemppainen, K. Hwang, N. J. Jeon, J. Seo, *Nat. Commun.* **2020**, *11*, 5146.
[66] H. Tsai, W. Nie, J.-C. Blancon, C. C. Stoumpos, R. Asadpour, B. Harutyunyan, A. J. Neukirch, R. Verduzco, J. J. Crochet, S. Tretiak, L. Pedesseau, J. Even, M. A. Alam, G. Gupta, J. Lou, P. M. Ajayan, M. J. Bedzyk, M. G. Kanatzidis, A. D. Mohite, *Nature* **2016**, *536*, 312.
[67] D. Angmo, G. DeLuca, A. D. Scully, A. S. R. Chesman, A. Seeber, C. Zuo, D. Vak, U. Bach, M. Gao, *Cell Rep.* **2021**, *2*, 100293.
[68] H. Min, D. Y. Lee, J. Kim, G. Kim, K. S. Lee, J. Kim, M. J. Paik, Y. K. Kim, K. S. Kim, M. G. Kim, T. J. Shin, S. Il Seok, *Nature* **2021**, *598*, 444.
[69] N. K. Noel, M. Congiu, A. J. Ramadan, S. Fearn, D. P. Mcmeekin, J. B. Patel, M. B. Johnston, B. Wenger, H. J. Snaith, *Joule* **2017**, *1*, 328.
[70] Y. Chen, N. Li, L. Wang, L. Li, Z. Xu, H. Jiao, P. Liu, C. Zhu, H. Zai, M. Sun, W. Zou, S. Zhang, G. Xing, X. Liu, J. Wang, D. Li, B. Huang, Q. Chen, H. Zhou, *Nat. Commun.* **2019**, *10*, 1112.
[71] J.-W. Lee, H.-S. Kim, N.-G. Park, *Acc. Chem. Res.* **2016**, *49*, 311.
[72] J. C. Hamill Jr., J. Schwartz, Y.-L. Loo, *ACS Energy Lett.* **2018**, *3*, 92.
[73] Y. Zhao, P. Zhu, M. Wang, S. Huang, Z. Zhao, S. Tan, T.-H. Han, J.-W. Lee, T. Huang, R. Wang, J. Xue, D. Meng, Y. Huang, J. Marian, J. Zhu, Y. Yang, *Adv. Mater.* **2020**, *32*, 1907769.
[74] E. Aydin, M. De Bastiani, S. De Wolf, *Adv. Mater.* **2019**, *31*, 1900428.
[75] B. Chen, P. N. Rudd, S. Yang, Y. Yuan, J. Huang, *Chem. Soc. Rev.* **2019**, *48*, 3842.
[76] Y. Li, H. Wu, W. Qi, X. Zhou, J. Li, J. Cheng, Y. Zhao, Y. Li, X. Zhang, *Nano Energy* **2020**, *77*, 105237.
[77] J. M. Ball, A. Petrozza, *Nat. Energy* **2016**, *1*, 16149.
[78] J. Warby, F. Zu, S. Zeiske, E. Gutierrez-Partida, L. Frohloff, S. Kahmann, K. Frohna, E. Mosconi, E. Radicchi, F. Lang, S. Shah, F. Peña-Camargo, H. Hempel, T. Unold, N. Koch, A. Armin, F. De Angelis, S. D. Stranks, D. Neher, M. Stolterfoht, *Adv. Energy Mater.* **2022**, *12*, 2103567.
[79] A. Al-Ashouri, E. Köhnen, B. Li, A. Magomedov, H. Hempel, P. Caprioglio, J. A. Márquez, A. B. Morales Vilches, E. Kasparavicius, J. A. Smith, N. Phung, D. Menzel, M. Grischek, L. Kegelmann, D. Skroblin, C. Gollwitzer, T. Malinauskas, M. Jost, G. Matic, B. Rech, R. Schlatmann, M. Topic, L. Korte, A. Abate, B. Stannowski, D. Neher, M. Stolterfoht, T. Unold, V. Getautis, S. Albrecht, *Science* **2020**, *370*, 1300.
[80] M. Stolterfoht, C. M. Wolff, J. A. Márquez, S. Zhang, C. J. Hages, D. Rothhardt, S. Albrecht, *Nat. Energy* **2018**, *3*, 847.
[81] L. Rakocevic, R. Gehlhaar, T. Merckx, W. Qiu, U. W. Paetzold, H. Fledderus, J. Poortmans, *IEEE J. Photovoltaics* **2017**, *7*, 404.
[82] Y. Xu, S. Wang, L. Gu, N. Yuan, J. Ding, *Sol. RRL* **2021**, *5*, 2000733.
[83] B. Wilkinson, N. L. Chang, M. A. Green, A. W. Y. Ho-Baillie, *Prog. Photovoltaics* **2018**, *26*, 659.
[84] S.-J. Moon, J.-H. Yum, L. Lofgren, A. Walter, L. Sansonnens, M. Benkhaira, S. Nicolay, J. Bailat, C. Ballif, *IEEE J. Photovoltaics* **2015**, *5*, 1087.
[85] A. L. Palma, F. Matteocci, A. Agresti, S. Pescetelli, E. Calabro, L. Vesce, S. Christiansen, M. Schmidt, A. Di Carlo, *IEEE J. Photovoltaics* **2017**, *7*, 1674.
[86] K. G. Brooks, M. K. Nazeeruddin, *Adv. Energy Mater.* **2021**, *11*, 2101149.
[87] A. L. Palma, *Sol. RRL* **2020**, *4*, 1900432.
[88] B. Dou, J. B. Whitaker, K. Bruening, D. T. Moore, L. M. Wheeler, J. Ryter, N. J. Breslin, J. J. Berry, S. M. Garner, F. S. Barnes, S. E. Shaheen, C. J. Tassone, K. Zhu, M. F. A. M. van Hest, *ACS Energy Lett.* **2018**, *3*, 2558.
[89] C. Wu, K. Wang, J. Li, Z. Liang, J. Li, W. Li, L. Zhao, B. Chi, S. Wang, *Matter* **2021**, *4*, 775.
[90] X. Chen, Y. Xia, Q. Huang, Z. Li, A. Mei, Y. Hu, T. Wang, R. Cheacharoen, Y. Rong, H. Han, *Adv. Energy Mater.* **2021**, *11*, 2100292.
[91] J. Troughton, C. Charbonneau, M. J. Carnie, M. L. Davies, D. A. Worsley, T. M. Watson, *J. Mater. Chem. A* **2015**, *3*, 9123.
[92] T. Druffel, R. Dharmadasa, B. W. Lavery, K. Ankireddy, *Sol. Energy Mater. sol. Cells* **2018**, *174*, 359.
[93] N. Rolston, W. J. Scheideler, A. C. Flick, J. P. Chen, H. Elmaraghi, A. Sleugh, O. Zhao, M. Woodhouse, R. H. Dauskardt, *Joule* **2020**, *4*, 2675.
[94] X. Zheng, Z. Li, Y. Zhang, M. Chen, T. Liu, C. Xiao, D. Gao, J. B. Patel, D. Kuciauskas, A. Magomedov, R. A. Scheidt, X. Wang, S. P. Harvey, Z. Dai, C. Zhang, D. Morales, H. Pruett, B. M. Wieliczka, A. R. Kirmani, N. P. Padture, K. R. Graham, Y. Yan, M. K. Nazeeruddin, M. D. Mcgehee, Z. Zhu, J. M. Luther, *Nat. Energy* **2023**, *8*, 462.
[95] D. Bi, W. Tress, M. I. Dar, P. Gao, J. Luo, C. Renevier, K. Schenk, A. Abate, F. Giordano, J.-P. Correa Baena, J.-D. Decoppet, S. M. Zakeeruddin, M. K. Nazeeruddin, M. Grätzel, A. Hagfeldt, *Sci. Adv.* **2016**, *2*, e1501170.
[96] W. Luo, Y. S. Khoo, P. Hacke, V. Naumann, D. Lausch, S. P. Harvey, J. P. Singh, J. Chai, Y. Wang, A. G. Aberle, S. Ramakrishna, *Energy Environ. Sci.* **2017**, *10*, 43.
[97] H. J. Snaith, P. Hacke, *Nat. Energy* **2018**, *3*, 459.
[98] Z. Zhang, H. Wang, T. J. Jacobsson, J. Luo, *Nat. Commun.* **2022**, *13*, 7639.
[99] C. C. Boyd, R. Cheacharoen, T. Leijtens, M. D. Mcgehee, *Chem. Rev.* **2019**, *119*, 3418.
[100] J.-W. Lee, N.-G. Park, *Adv. Energy Mater.* **2020**, *10*, 1903249.
[101] J. Zhao, Y. Deng, H. Wei, X. Zheng, Z. Yu, Y. Shao, J. E. Shield, J. Huang, *Sci. Adv.* **2017**, *3*, eaao5616.
[102] X. Liu, D. Luo, Z.-H. Lu, J. S. Yun, M. Saliba, S. I. Seok, W. Zhang, *Nat. Rev. Chem.* **2023**, *7*, 462.
[103] W. Fu, A. G. Ricciardulli, Q. A. Akkerman, R. A. John, M. M. Tavakoli, S. Essig, M. V. Kovalenko, M. Saliba, *Mater. Today* **2022**, *58*, 275.
[104] L. Nakka, Y. Cheng, A. G. Aberle, F. Lin, *Adv. Energy Sustainability Res.* **2022**, *3*, 2200045.
[105] L. Zhao, R. A. Kerner, Z. Xiao, Y. L. Lin, K. M. Lee, J. Schwartz, B. P. Rand, *ACS Energy Lett.* **2016**, *1*, 595.
[106] Z. Liu, L. Qiu, L. K. Ono, S. He, Z. Hu, M. Jiang, G. Tong, Z. Wu, Y. Jiang, D.-Y. Son, Y. Dang, S. Kazaoui, Y. Qi, *Nat. Energy* **2020**, *5*, 596.
[107] Y. Wang, I. Ahmad, T. Leung, J. Lin, W. Chen, F. Liu, A. M. C. Ng, Y. Zhang, A. B. Djurisic, *ACS Mater Au* **2022**, *2*, 215.

[108] Y. Bai, Y. Zhao, J. Li, H. Chen, A. Lambertz, Q. Qiu, C. Qian, J. Shi, W. Liu, T. Chen, J. Yu, K. Ding, J. Yu, *Energy Technol.* **2023**, *11*, 2201466.
[109] M. De Bastiani, M. Babics, E. Aydin, A. S. Subbiah, L. Xu, S. De Wolf, *Sol. RRL* **2022**, *6*, 2100493.
[110] L. Shi, M. P. Bucknall, T. L. Young, M. Zhang, L. Hu, J. Bing, D. S. Lee, J. Kim, T. Wu, N. Takamure, D. R. Mckenzie, S. Huang, M. A. Green, A. W. Y. Ho-Baillie, *Science* **2020**, *368*, eaba2412.
[111] S. Ahmed, S. Li, Z. Li, G. Xiao, T. Ma, *Appl. Energy* **2022**, *308*, 118363.
[112] N. Xu, P. Zhu, Y. Sheng, L. Zhou, X. Li, H. Tan, S. Zhu, J. Zhu, *Joule* **2020**, *4*, 347.
[113] E. Bi, W. Tang, H. Chen, Y. Wang, J. Barbaud, T. Wu, W. Kong, P. Tu, H. Zhu, X. Zeng, J. He, S.-I. Kan, X. Yang, M. Grätzel, L. Han, *Joule* **2019**, *3*, 2748.
[114] K. A. Bush, C. D. Bailie, Y. Chen, A. R. Bowring, W. Wang, W. Ma, T. Leijtens, F. Moghadam, M. D. Mcgehee, *Adv. Mater.* **2016**, *28*, 3937.
[115] S. Hong, H. Kang, G. Kim, S. Lee, S. Kim, J.-H. Lee, J. Lee, M. Yi, J. Kim, H. Back, J.-R. Kim, K. Lee, *Nat. Commun.* **2016**, *7*, 10279.
[116] J.-W. Lee, S. Tan, S. I. Seok, Y. Yang, N.-G. Park, *Science* **2022**, *375*, eabj1186.
[117] E. J. Wolf, I. E. Gould, L. B. Bliss, J. J. Berry, M. D. Mcgehee, *Sol. RRL* **2022**, *6*, 2100239.
[118] D. Lan, M. A. Green, *Joule* **2022**, *6*, 1782.
[119] A. R. Bowring, L. Bertoluzzi, B. C. O'regan, M. D. Mcgehee, *Adv. Energy Mater.* **2018**, *8*, 1702365.
[120] A. Ndiaye, A. Charki, A. Kobi, C. M. F. Kébé, P. A. Ndiaye, V. Sambou, *Sol. Energy* **2013**, *96*, 140.
[121] I. Mathews, S. Sofia, E. Ma, J. Jean, H. S. Laine, S. C. Siah, T. Buonassisi, I. M. Peters, *Joule* **2020**, *4*, 822.
[122] N. Rolston, A. D. Printz, J. M. Tracy, H. C. Weerasinghe, D. Vak, L. J. Haur, A. Priyadarshi, N. Mathews, D. J. Slotcavage, M. D. Mcgehee, R. E. Kalan, K. Zielinski, R. L. Grimm, H. Tsai, W. Nie, A. D. Mohite, S. Gholipour, M. Saliba, M. Grätzel, R. H. Dauskardt, *Adv. Energy Mater.* **2018**, *8*, 1702116.
[123] B. L. Watson, N. Rolston, K. A. Bush, L. Taleghani, R. H. Dauskardt, *J. Mater. Chem. A* **2017**, *5*, 19267.
[124] B. L. Watson, N. Rolston, A. D. Printz, R. H. Dauskardt, *Energy Environ. Sci.* **2017**, *10*, 2500.
[125] Z. Purohit, W. Song, J. Carolus, H. Chaliyawala, S. Lammar, T. Merckx, T. Aernouts, B. Tripathi, M. Daenen, *Sol. RRL* **2021**, *5*, 2100349.
[126] J. Carolus, T. Merckx, Z. Purohit, B. Tripathi, H.-G. Boyen, T. Aernouts, W. De Ceuninck, B. Conings, M. Daenen, *Sol. RRL* **2019**, *3*, 1900226.
[127] M. Cai, Y. Wu, H. Chen, X. Yang, Y. Qiang, L. Han, *Adv. Sci.* **2017**, *4*, 1600269.
[128] N. L. Chang, A. W. Yi Ho-Baillie, P. A. Basore, T. L. Young, R. Evans, R. J. Egan, *Prog. Photovoltaics* **2017**, *25*, 390.
[129] Z. Song, C. L. Mcelvany, A. B. Phillips, I. Celik, P. W. Krantz, S. C. Watthage, G. K. Liyanage, D. Apul, M. J. Heben, *Energy Environ. Sci.* **2017**, *10*, 1297.
[130] Z. Li, Y. Zhao, X. Wang, Y. Sun, Z. Zhao, Y. Li, H. Zhou, Q. Chen, *Joule* **2018**, *2*, 1559.
[131] R. Charles, A. Doolin, R. G. Rodriguez, K. V. Villalobos, M. L. Davies, *Environ. Sci.* **2023**, *16*, 3711.
[132] A. Halbe, K. Sharpe, G. Housser, D. Metacarpa, P. Haldar, presented at IEEE 42nd Photovoltaic Specialist Conference (PVSC), New Orleans, LA, USA, June **2015**, 1.
[133] D. Metacarpa, D. Fobare, A. Garney, F. Yan, D. Dwyer, E. Holton, P. Haldar, presented at *IEEE 42nd Photovoltaic Specialist Conference (PVSC)*, New Orleans, LA, USA, June **2015**, 1.
[134] L. Wagner, J. Suo, B. Yang, D. Bogachuk, E. Gervais, R. Pietzcker, A. Gassmann, J. C. Goldschmidt, The Resource Demand of Terawatt-Scale Perovskite Tandem Photovoltaics. **2023**, arXiv preprint, arXiv:2306.13375.
[135] N.-G. Park, M. Grätzel, T. Miyasaka, K. Zhu, K. Emery, *Nat. Energy* **2016**, *1*, 16152.
[136] S.-Y. Bae, S. Y. Lee, J.-W. Kim, H. N. Umh, J. Jeong, S. Bae, J. Yi, Y. Kim, J. Choi, *Sci. Rep.* **2019**, *9*, 4242.
[137] N. Moody, S. Sesena, D. W. Dequilettes, B. D. Dou, R. Swartwout, J. T. Buchman, A. Johnson, U. Eze, R. Brenes, M. Johnston, C. L. Haynes, V. Bulovic, M. G. Bawendi, *Joule* **2020**, *4*, 970.
[138] J. Li, H.-L. Cao, W.-B. Jiao, Q. Wang, M. Wei, I. Cantone, J. Lü, A. Abate, *Nat. Commun.* **2020**, *11*, 310.
[139] Y. Jiang, L. Qiu, E. J. Juarez-Perez, L. K. Ono, Z. Hu, Z. Liu, Z. Wu, L. Meng, Q. Wang, Y. Qi, *Nat. Energy* **2019**, *4*, 585.
[140] R. Vidal, J.-A. Alberola-Borràs, S. N. Habisreutinger, J.-L. Gimeno-Molina, D. T. Moore, T. H. Schloemer, I. Mora-Seró, J. J. Berry, J. M. Luther, *Nat. Sustainability* **2021**, *4*, 277.
[141] J. Gong, S. B. Darling, F. You, *Energy Environ. Sci.* **2015**, *8*, 1953.
[142] X. Tian, S. D. Stranks, F. You, *Nat. Sustainability* **2021**, *4*, 821.
[143] R. Vidal, J.-A. Alberola-Borràs, N. Sánchez-Pantoja, I. Mora-Seró, *Adv. Energy Sustainability Res.* **2021**, *2*, 2000088.
[144] G. Rodriguez-Garcia, E. Aydin, S. De Wolf, B. Carlson, J. Kellar, I. Celik, *ACS Sustainable Chem. Eng.* **2021**, *9*, 15239.
[145] B. Chen, C. Fei, S. Chen, H. Gu, X. Xiao, J. Huang, *Nat. Commun.* **2021**,*12*, 5859.
[146] K. Wang, T. Ye, X. Huang, Y. Hou, J. Yoon, D. Yang, X. Hu, X. Jiang, C. Wu, G. Zhou, S. Priya, *Matter* **2021**, *4*, 2522.
[147] S. Chen, Y. Deng, X. Xiao, S. Xu, P. N. Rudd, J. Huang, *Nat. Sustainability* **2021**, *4*, 636.
[148] H.-S. Yun, H. W. Kwon, M. J. Paik, S. Hong, J. Kim, E. Noh, J. Park, Y. Lee, S. Il Seok, *Nat. Energy* **2022**, *7*, 828.
[149] W. Hui, L. Chao, H. Lu, F. Xia, Q. Wei, Z. Su, T. Niu, L. Tao, B. Du, D. Li, Y. Wang, H. Dong, S. Zuo, B. Li, W. Shi, X. Ran, P. Li, H. Zhang, Z. Wu, C. Ran, L. Song, G. Xing, X. Gao, J. Zhang, Y. Xia, Y. Chen, W. Huang, *Science* **2021**, *371*, 1359.
[150] L. A. Zafoschnig, S. Nold, J. C. Goldschmidt, *IEEE J. Photovoltaics* **2020**, *10*, 1632.
[151] L. Duan, D. Walter, N. Chang, J. Bullock, D. Kang, S. P. Phang, K. Weber, T. White, D. Macdonald, K. Catchpole, H. Shen, *Nat. Rev. Mater.* **2023**, *8*, 261.
[152] B. Chen, Z. J. Yu, S. Manzoor, S. Wang, W. Weigand, Z. Yu, G. Yang, Z. Ni, X. Dai, Z. C. Holman, J. Huang, *Joule* **2020**, *4*, 850.
[153] C. Ballif, F.-J. Haug, M. Boccard, P. J. Verlinden, G. Hahn, *Nat. Rev. Mater.* **2022**, *7*, 597.

Pengchen Zhu obtained his B.S. degree in Materials Physics from Nanjing University in 2015 and his Ph.D. degree in Materials Science and Engineering from Nanjing University in 2020. He is currently an assistant professor in the School of Sustainable Energy and Resources at Nanjing University, where his research is focused on perovskite-related optoelectronic devices and interfacial photothermal manipulation.

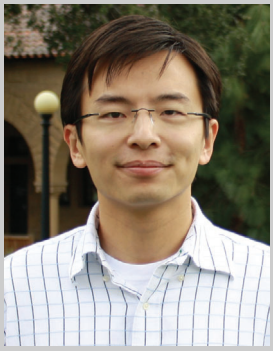

Jia Zhu received his B.S. degree in Physics from Nanjing University in China in 2003 and his M.S. and Ph.D. degrees in Electrical Engineering from Stanford University in 2006 and 2010, respectively. He went on to work as a postdoctoral scholar at the University of California, Berkeley. In 2013, he became a professor in the College of Engineering and Applied Sciences at Nanjing University. Now he is a Professor and the Dean of the School of Sustainable Energy and Resources at Nanjing University. He leads a group of researchers working on nanomaterials for energy conversion and storage.